Summer 2015

A force feedback haptic interface for atomic force microscopy

Abdulmohsen Alabdulmuhsin

Department:

A FORCE FEEDBACK HAPTIC INTERFACE FOR ATOMIC FORCE MICROSCOPY

by

ABDULMOHSEN ALABDULMUHSIN

A THESIS

Presented to the Faculty of the Graduate School of the

MISSOURI UNIVERSITY OF SCIENCE AND TECHNOLOGY

In Partial Fulfillment of the Requirements for the Degree

MASTER OF SCIENCE IN MECHANICAL ENGINEERING

2015

Approved by

Douglas A. Bristow, Advisor
Robert G. Landers
S. N. Balakrishnan

ABSTRACT

Integrating a force feedback haptic device with atomic force microscopy (AFM) improves the capability to investigate and manipulate the objects on a micro- and nanoscale surface. The haptic device provides the researcher with a sense of touch and movement by changing the position of the stylus or amount of force on it. The developed system's concept is to provide the user a sense and feel and control of the AFM probe at the nanoscale. By positing the haptic stylus, the user generates reference to commands to the AFM probe. In turn, forces experienced by the probe are communicated to the haptic and transferred to the user. In order to ensure that the forces that act on the haptic and the probe are accurate, it is important to calibrate the normal and lateral forces that act on the tip of the probe. These forces are generated due to using a contact mode interaction between the probe tip and the sample surface. The haptic-probe coupled motion is tested to reach the desired results. Also, a low pass filter is used to remove the undesirable high frequency content from the input force to the haptic since it affects the interaction between the probe's tip and the sample's surface. To close, the sensitivities of haptic to the probe position, and displacement of the probe to the force on the haptic are discussed.

ACKNOWLEDGMENTS

I would like to express my sincere thanks to my advisor, Dr. Douglas Bristow, for the continuous support, patience and guidance throughout my research work. Without his guidance and enthusiasm this work would not have occurred.

I would like to thank Professors S. N. Balakrishnan and Robert Landers for serving on my thesis committee. I thank my fellow lab members of Precision Motion Control Laboratory (PMCLab), especially Muthukumaran Loganathan and Ayad Al-Ogaidi for their assistance and help. A special thanks to Muthukumaran for providing his perception about the AFM.

Last but not the least, I would like to thank my family I would not have made it without them.

TABLE OF CONTENTS

Page

LIST OF ILLUSTRATIONS

LIST OF TABLES

1. INTRODUCTION

Atomic force microscopy (AFM) is an essential tool for nanotechnology researchers. The use of the AFM allows material to be imaged and manipulated at nanoscale precision. The process involves scanning an object, manipulating the object, and then scanning the object again to confirm that the manipulation(s) have produced the desired results. The entire process is time consuming and requires great effort. A force-feedback haptic device improves on the process by allowing the researcher to feel the surface of the material as scanning and manipulation occurs allowing for a more efficient touch-based manipulation.

1.1. ATOMIC FORCE MICROSCOPY

In 1986, Binnig invented the atomic force microscopy [1] to increase the ways that different materials such as conductors and insulators can be examined at the nanoscale. An AFM allows researchers to investigate at the level of an angstrom, a measurement which is equal to 0.1 nanometers on the nano scale. Using microscopy to image a sample surface allows the roughness of a surface to be defined and can allow the properties of the material to be changed through manipulation.

The main component of the atomic force microscopy is shown in Figure 1.1. During AFM, a laser is pointed at the probe (cantilever), to allow the detector to identify any change in probe position. Moving the stage or the probe while the tip of the probe is touching the sample surface will cause a change in the laser point on the detector due to the bending or twisting of the probe.

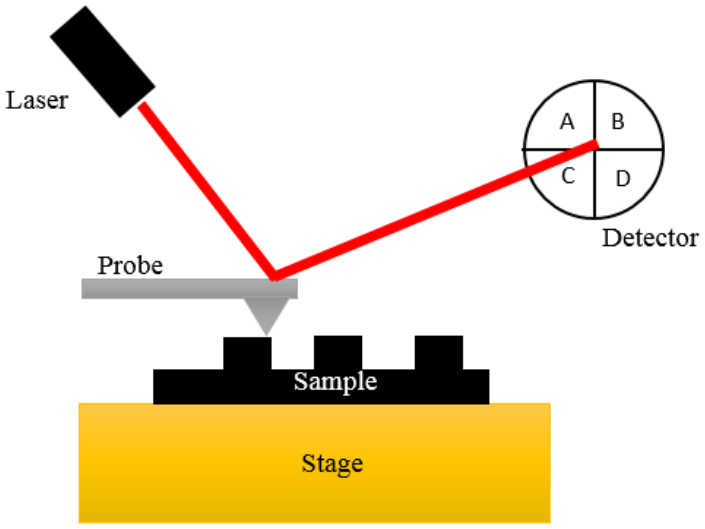

Figure 1.1 Schematic of Atomic force microscopy

1.2. FORCE FEEDBACK HAPTIC

A force feedback haptic device is a mechanical device that provides a user with a sense of touch and movement by changing the position or amount of force. It is used as a tele-robotic system to provide the user with a virtual environment. In 1964, Mosher [2], 1968 Corliss [3], and 1983 Thring [4] created methods of designing a force feedback haptic device. Haptic devices have many applications such as in simulator systems, tele-operator systems, video games, mobile devices, and virtual reality environments.

1.3. HAPTIC-AFM INTERFACE

Sitti, 1998 [5] and Guthold, 2000 [6] developed a force feedback haptic device as an interface with AFM. Li, 2004 [7] developed the first real-time nanomanipulator by interfacing the haptic with AFM. In this thesis, a force feedback haptic device is interfaced with custom AFM.

The haptic is used to interface with AFM system in this thesis is the Geomagic® Touch™ X Haptic Device. This device was created as a result of the research of Massie, 1993 [8]. This haptic is interfaced with the AFM located in the Precision Motion Control Laboratory (PMCLab) at the Missouri University of Science and Technology.

The system's concept is shown in Figure 1.2 and provides the user with a sense and the feel of the nano scale in the probe of the AFM using the haptic device. The user applies force to change the haptic position in one scale and the device changes the probe in a nano scale. This change applies a nano scale force on the probe which has been scaled to the user's needs through the haptic so that the user can feel the same direction of the force on the probe.

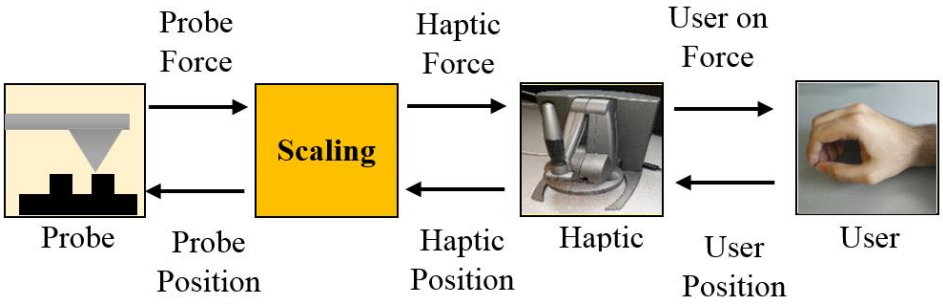

Figure 1.2 Concept of the haptic-AFM interface

1.4. RESEARCH OBJECTIVE

The need to perform accurate manipulation in the micro- and nanoscale continues to grow. The uses of these manipulations include achieving material geometrics, especially 3D geometrics, in the micro or nano scale. These tasks to be performed in an explorative or manipulative capacity by enhancing the AFM. This thesis works to improve the AFM's capability to investigate and manipulate objects on a micro- and nanoscale surface by integrating a force feedback haptic device for AFM using contact mode. This technique includes programing the haptic to control the cantilever movement and to sense the force from the cantilever's tip. Calibrating and filtering the system signal is also explored.

2. LITERATURE REVIEW

This chapter includes a literature review of the forces impacting the cantilever of the AFM and the development of AFM integrated with haptic device. Section 2.1 provides a review of the forces acting on the tip of the cantilever as a result of moving the probe above the sample surface. Ways of integrating a force feedback haptic device with atomic force microscopy is reviewed in Section 2.2.

2.1. INTERACTION FORCES

The normal and lateral forces that act on the tip of the cantilever are shown in Figure 2.1. Prior to developing a haptic user interface with AFM, these forces must be properly understood through the use of a thorough study and review of the literature regarding these forces without regard to attractive and repulsive forces [7, 9]. The normal and lateral forces must be calibrated before they are sent to the haptic [3].

2.1.1. Tip Forces. The best approach to calculate tip forces is found in [7] [9]. These forces can be identified using Hooke's law which calculates force using the spring constant (k) and the amount of deflection (Δx)

$$F = k\Delta x \tag{1}$$

So, from Figure 2.1 the force in normal direction is,

$$F_n = k\delta_z \tag{2}$$

where the k is the spring constant of the cantilever, and δ_z is change in position in z direction (bending).

The force from the lateral direction is,

$$F_l = \frac{k_l}{h}\theta_x \tag{3}$$

where k_l is the torsional constant, h is the cantilever tip height, and the θ_x is the change in x axis angle due to the lateral force (twist).

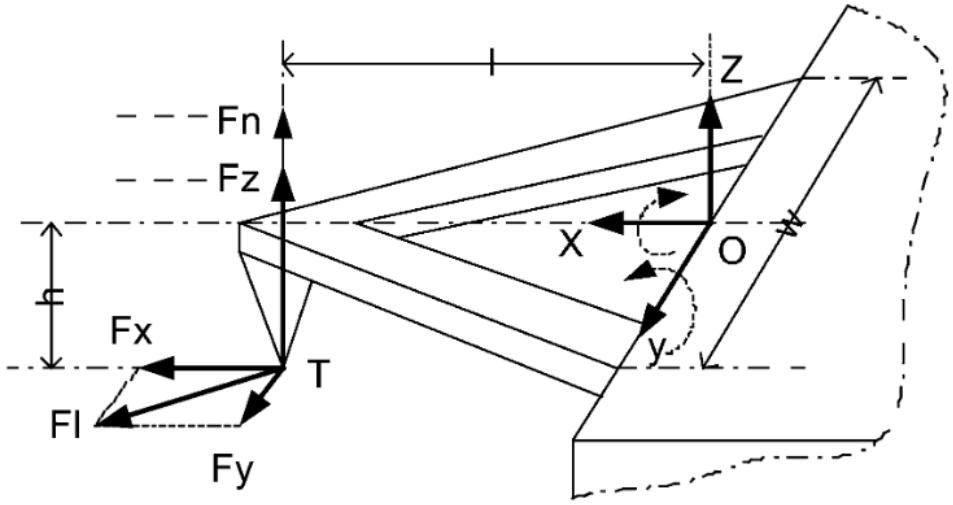

Figure 2.1 Force analysis of an AFM cantilever where O point is the origin of the cantilever frame [7]

To calculate the force on the tip apex. The F_x, F_y, and F_z act on point O in Figure 2.1 as τ_x, τ_y, and τ_z [7, 9]. The XYZ torques can be calculated as,

$$\tau_x = F_y h \tag{4}$$

$$\tau_y = -F_z l - F_x h \tag{5}$$

$$\tau_z = F_y l \tag{6}$$

where l is the cantilever length. θ_x is generated from τ_x, δ_z is produced from τ_y, and δ_z can be neglected from τ_z since it is very small deflection [7, 9].

To calculate the forces, the δ_z and θ_x should be found first. To find these parameters, a photodiode is used to measure these values as shown in Figure 2.2 as,

$$S_n = \frac{(A+B)-(C+D)}{A+B+C+D} \tag{7}$$

$$S_l = \frac{(A+C)-(B+D)}{A+B+C+D} \tag{8}$$

where S_n is the normal photodiode signal, and S_l is the lateral photodiode signal. To relate equation (5) with (7) and equation (6) with (8), the normal and lateral gains (K_n and K_l) are added and should be calibrated for each AFM (see Section 2.1.2)

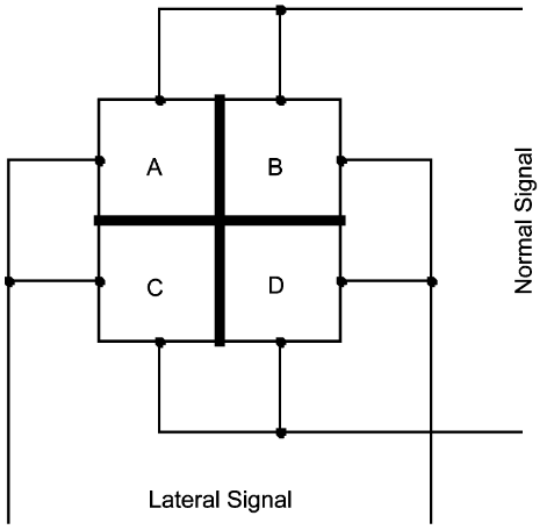

Figure 2.2 Photodiode detector. A, B, C, and D are signal output [9]

$$\delta_z = K_n S_n \tag{9}$$

$$\theta_x = K_l S_l \tag{10}$$

Therefore, the combination of equation (2) with (9) and equation (3) with (10) become

$$F_n = kK_n S_n \tag{11}$$

$$F_l = \frac{k_l}{h} K_l S_l \tag{12}$$

To find the relationship between the normal and lateral forces with the XYZ forces based on Figure 2.1,

$$F_n = -\frac{\tau_y}{l} = F_z + \frac{h}{l} F_x \tag{13}$$

$$F_y = \frac{k_l}{h} \theta_x = \frac{k_l K_l}{h} S_l \tag{14}$$

$$F_l = \frac{F_y}{\sin(\phi)} \tag{15}$$

$$F_x = F_y \tan(\phi) \tag{16}$$

where φ is the angle between the tip motion in XY plane with respect to the X-axis. A problem arises when the φ is zero and there is no motion in the Y axis. When this occurs, it will make equations (15) and (16) unmeasurable. To avoid this case, the angle of motion in XY plane should be bounded [9]. Based on the above equations, the XYZ forces can be written as

$$F_y = \frac{k_l K_l}{h} S_l \tag{17}$$

$$F_x = -\frac{F_y}{\tan \varphi} \tag{18}$$

$$F_z = k K_n S_n - \frac{h}{l} F_x \tag{19}$$

Note: F_x should be calculated before calculations of F_x and then F_z.

2.1.2. Calibration. It is important to calibrate the forces on the tip precisely to ensure that the forces that act on the haptic and the cantilever are accurate. Equations (17),

(18), and (19) use k, the spring constant of the cantilever, something which is usually provided by the manufacturer. K_n is the normal force gained and can be found using the approach retract method to find the slope between the deflection in Z axis and the normal signal of the photodiode. Equation (9) defines K_n as

$$K_n = \frac{d\delta_z}{dS_n} \tag{9}$$

This approach is used in most of the calibration methods found in the literature to determine the normal gain to calculate the normal force on the tip of the cantilever [10]. The lateral gain, K_l, in (17) is very hard to find by itself [10]. Many approaches are used to calibrate this direction [11, 12, 13]. The approach in [10] is close to what has been used in [13], but in a simpler way. The approach uses a tilted sample to move the cantilever tip up and down on the surface as shown in Figure 2.3. This approach is used to calibrate the lateral direction for this thesis (see Section 4.1.2).

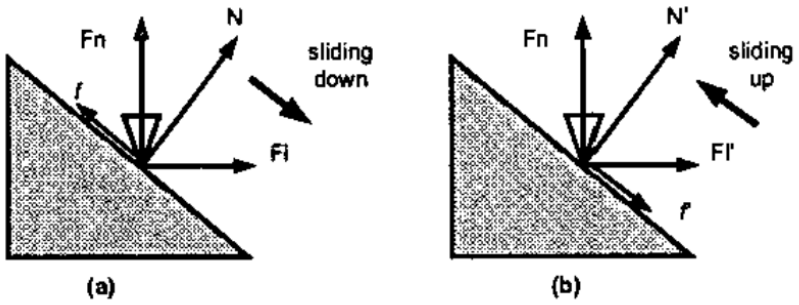

Figure 2.3 Force component from sliding the cantilever up and down on the tilted sample surface [10]

2.2. HAPTIC-AFM INTERFACE

A commercial haptic device is used to integrate the device with an AFM [14, 15, 16]. The specification of the haptic device can affect the result of interfacing the device with an AFM [14]. As shown in Figure 2.4, there are many different types of haptic devices including the workspace, maximum force, and position resolution.

Figure 2.4 (a) force feedback joystick, (b) Phantom Desktop, (c) Phantom Omni [14]

There are different set ups used to interface a specific type of AFM with a specific type of a haptic device. In approach [9], one of the first real-time haptic devices interfaced with an AFM. The interface used the capabilities of new technologies and had a super computer collect and control real-time data. The system configuration of approach [9] is shown in Figure 2.5.

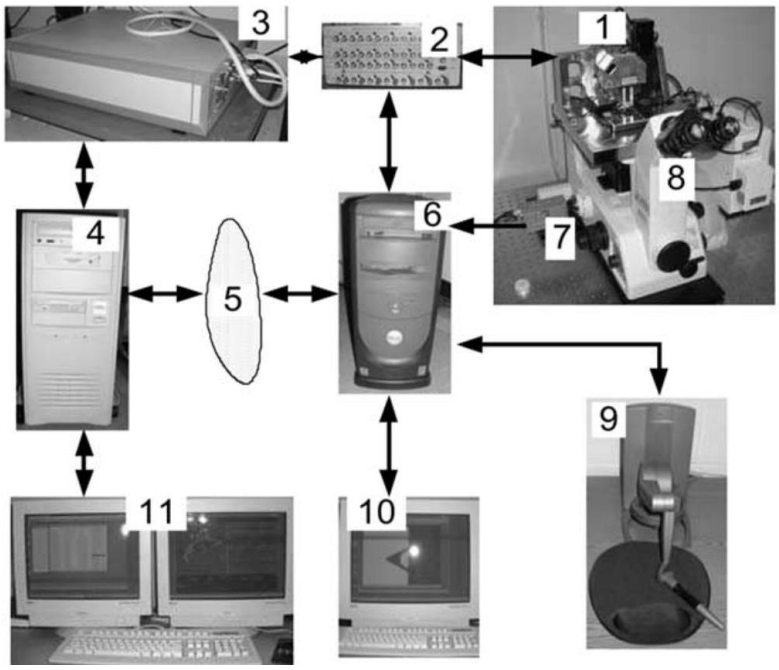

Figure 2.5 (1) AFM head, (2) Signal access module, (3) Controller, (4) Main computer, (5) Ethernet, (6) Second computer, (7) CCD camera, (8) Inverted optical microscope, (9) Phantom, (10) Single monitor, (11) Twin-monitor [9]

Approach [17], focuses on obtaining better imaging and graphics with real-time data as shown in Figure 2.6.

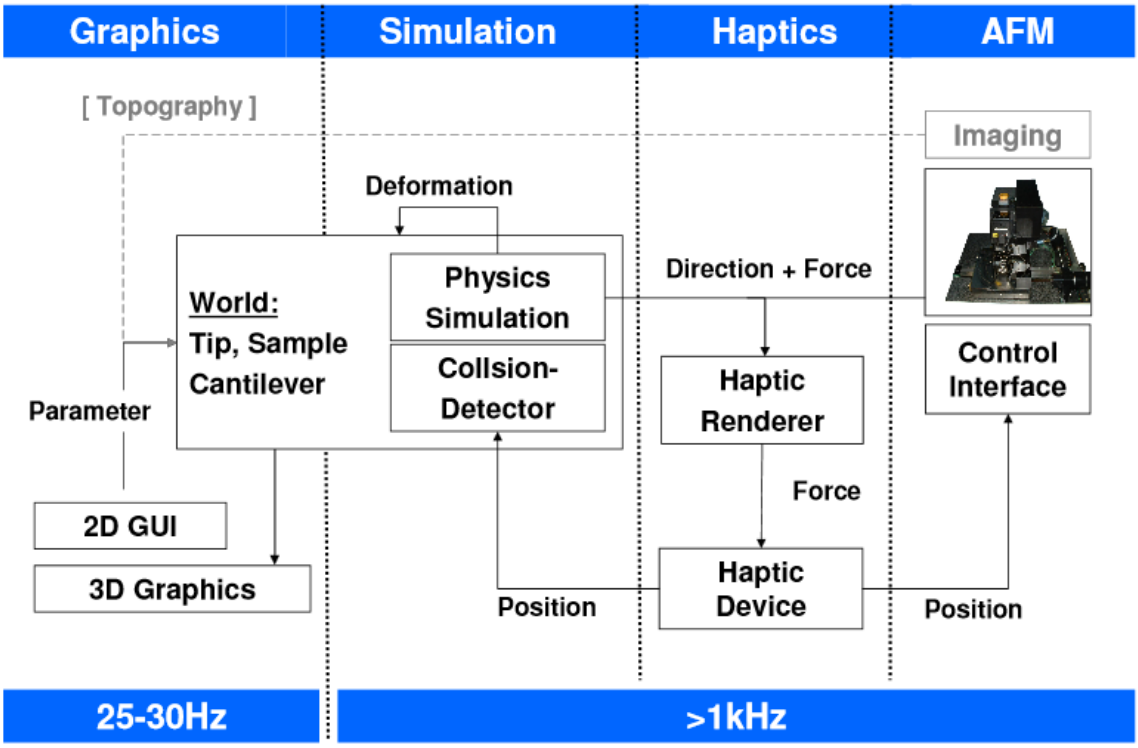

Figure 2.6 Haptic AFM system for simulation [17]

In approach [18], the AFM cantilever is used as adaptable end effector during manipulation. The adaptable end effector is controlled to maintain straight and that the control signal is shown on the haptic as force data [18]. Figure 2.7 shows the system setup.

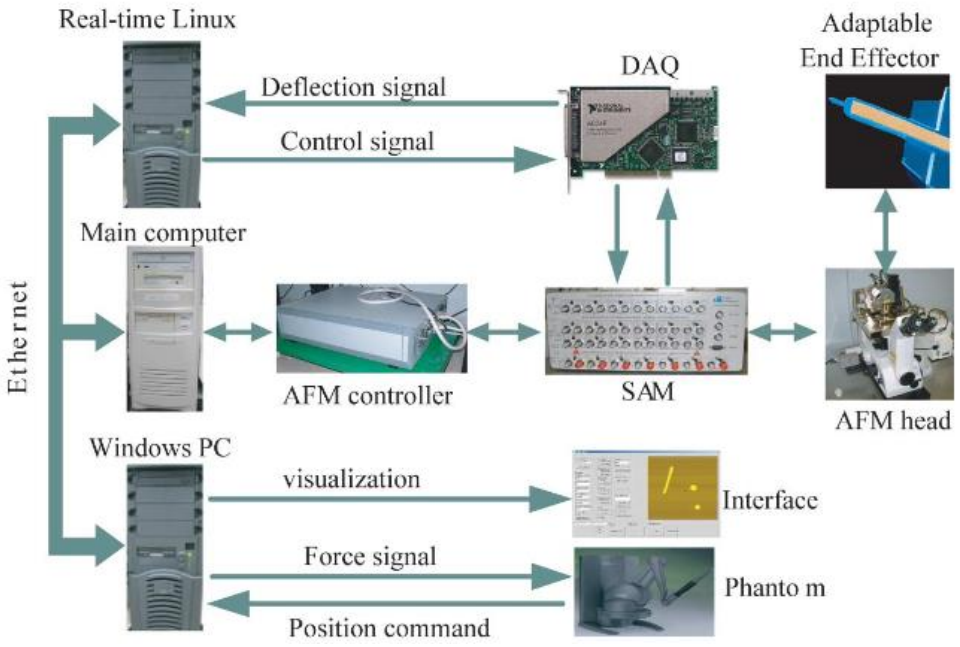

Figure 2.7 Set up of the haptic AFM system using adaptable end effector [18]

In approach [19], the haptic is used to make the user feel the change of the cantilever tip position while the probe is cutting the sample. The schematic diagram of the experimental set up of nanometer-scale manipulation and ultrasonic cutting using an atomic force microscope controlled by a haptic device is shown in Figure 2.8.

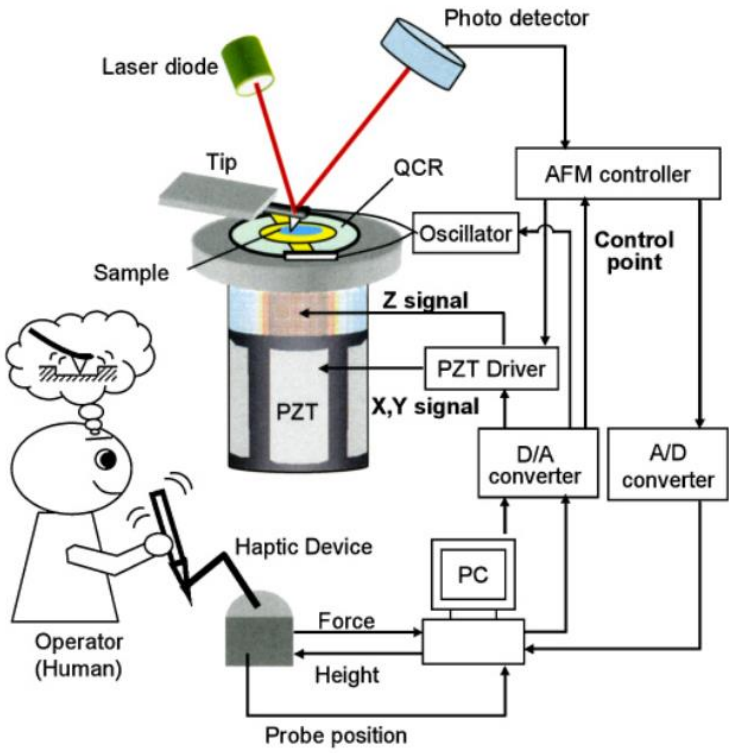

Figure 2.8 Schematic diagram of the experimental setup of an AFM with a nano manipulator and an ultrasonic nano-cutter [19]

3. METHODOLOGICAL DESIGN

Developing the haptic device interface for an AFM requires an understanding of the sample forces on the cantilever, the system hardware and software. There are two forces acting on the cantilever (i.e., normal and lateral) that will be transmitted to the user through the haptic. These forces will be explained on Section 3.1. The main AFM hardware components are shown in Figure 3.1: Micro Stage, Nano Stage, Sample, Photodiode detector, Laser, Mirror, and Picocube are mounted on vibration isolation table.

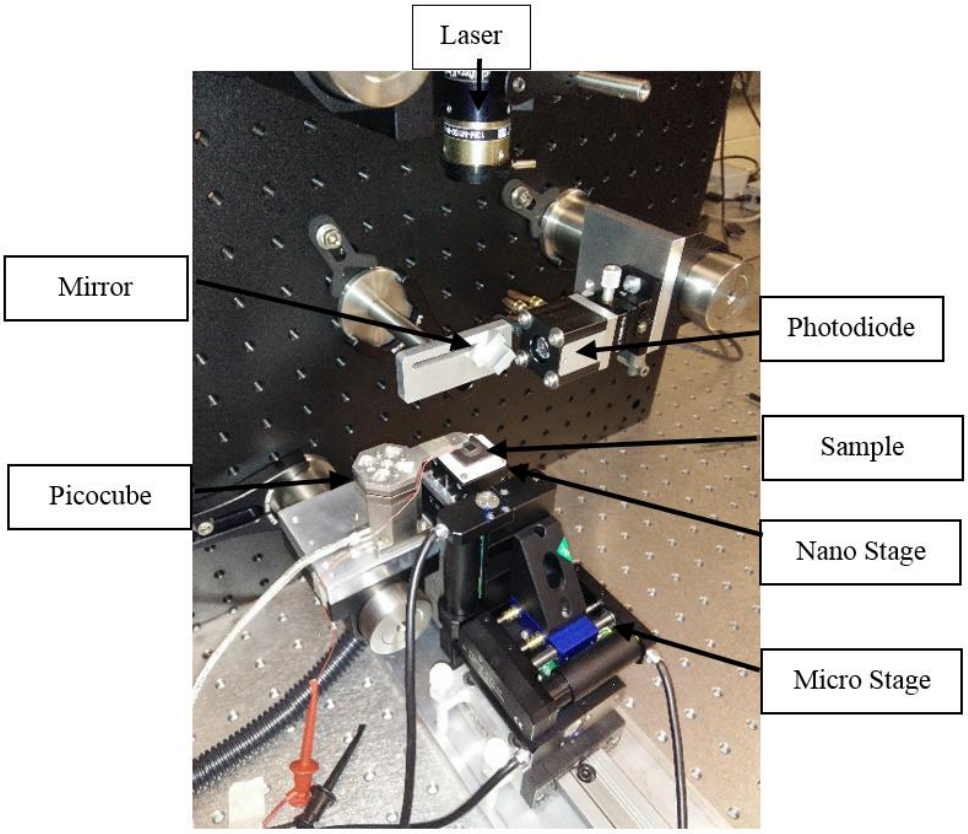

Figure 3.1 Photo of the main AFM components: Micro Stage, Nano Stage, Sample, Photodiode detector, Laser, Mirror, and Picocube

An M-112.1DG Compact Micro-Translation Stage from Physik Instrumente (PI) is used for AFM as a micro stage with 25 mm travel range and 0.05 μm resolution. Table 3.1 shows the technical data of the micro stage [20].

Table 3.1 Micro stage specifications [20]

Travel range	25 mm
Resolution	0.05 μm
Maximum velocity	1.5 mm/sec
Maximum holding force	10 N
Motor type	DC motor
Operating voltage	0 to ±12 V
Mass	0.3 Kg
Controller	C-863.11 Controller

A P-621.2CL PIHera XY Piezo Stage is used for the XY nano stage axes with 100 μm travel range and 0.4 nm resolution. Table 3.2 shows the technical data of the nano stage [21].

Table 3.2 Nano stage specifications [21]

Travel range XY	100 μm
Travel range Z	50 μm
Resolution	0.2 nm
Linearity:	0.02%
Load capacity	10 N
Mass	0.12 kg
Controller	E-500 Modular Piezo Controller

Also, A P-620.ZCL PIHera Precision Z-Stage for the Z axis with 50 μm travel range and 0.2 nm resolution. The picocube is P-363 PicoCube XYZ with 5 μm travel range and 0.1 nm resolution. Table 3.3 shows the technical data of the picocube [22].

Table 3.3 Picocube specifications [22]

Travel range	5 μm
resolution	0.1 nm
Linearity	0.05%
Load capacity	10 N
Mass	225 g
Controller	E-536 PicoCube Controller

3.1. FORCE ON THE CANTILEVER

The force acted on the tip of a cantilever using contact mode is due to moving the probe in three directions using the Cartesian coordinate as shown in Figure 3.2. Moving the cantilever in the Z direction generates a normal force F_n in N in the opposite direction on the cantilever causing a deflection in the Z direction by δ_z in nm. The lateral force F_l in N caused by the movement in the Y direction causes the cantilever to twist around X axis with θ_x in radian as shown in Figure 3.3. Deflections resulting from forces in the X direction are negligible because of the high stiffness of the cantilever in that direction [7].

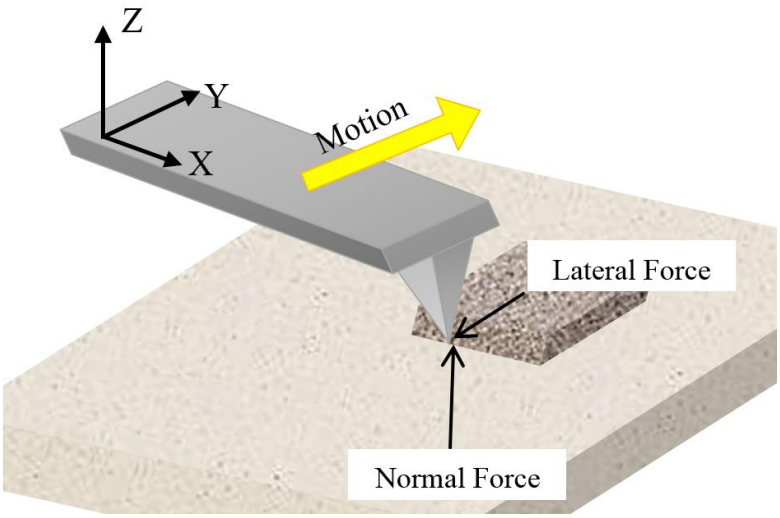

Figure 3.2 Schematic of forces on an AFM cantilever

The normal and lateral forces are derived from Hooke's law as,

$$F_n = k\delta_z \tag{1}$$

$$F_l = \frac{k_l}{h}\theta_x \tag{2}$$

where k is the cantilever spring constant in N / nm, k_l is the cantilever torsional spring constant in the lateral direction in N-nm / radian, and h is the tip height in nm as shown in Figure 3.3.

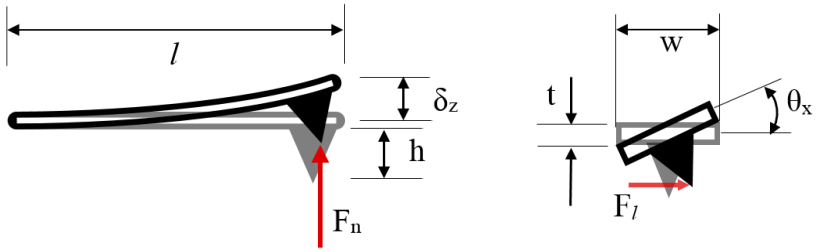

(a) (b)

Figure 3.3 Schematic of the effect of the forces on the tip of the cantilever, (a) bending motion from normal force F_n, and (b) torsional motion from lateral force F_l

The photodiode can detect the change of the cantilever position in Z direction as the change of the photodiode vertical signal in Volte as shown in Figure 3.4, V_V,

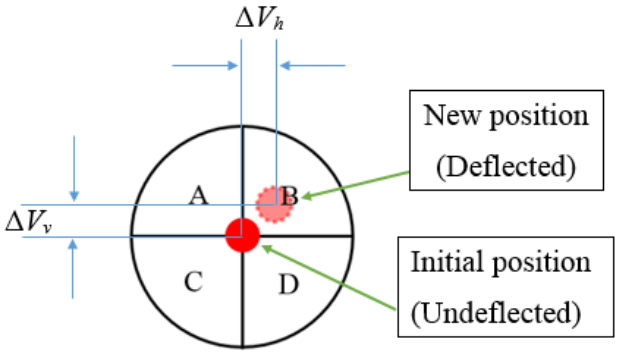

Figure 3.4 Schematic of the photodiode detector where A, B, C, and D are the voltages output from the photodiode

$$V_v = \frac{(A+B)-(C+D)}{A+B+C+D}, \tag{3}$$

and,

$$\delta_z = S_n V_v, \tag{4}$$

where A, B, C, D represent the voltage detected by the photodiodes in the quad-cell photodetector and S_n is the voltage sensitivity to be determined. The photodiode horizontal signal V_h can detect the twist θ_x as,

$$V_h = \frac{(A+C)-(B+D)}{A+B+C+D}, \tag{5}$$

and,

$$\theta_x = S_l V_h, \tag{6}$$

where S_l is the voltage sensitivity for the cantilever twist around the X axis.

Then, from (1) and (2) with (4) and (6) the normal and lateral force acted on the cantilever can be drive as:

$$F_n = kS_n V_v \tag{7}$$

$$F_l = \frac{k_l}{h} S_l V_h \tag{8}$$

3.2. HAPTIC INTEGRATION

The Geomagic Touch X (formerly Phantom Desktop), shown in Figure 3.5, is used as the force feedback haptic device. This haptic gives a precise position with 0.023 mm resolution, 160 mm width (Y_h) x 120 mm height (Z_h) x 120 mm depth (X_h) as force feedback workspace, 7.9 N maximum force, and the spring stiffness for XYZ axes are 1.86, 2.35, and 1.48 N/mm, respectively [23]. Inputs to the haptic device are six axes of stylus motion ($X_h\, Y_h\, Z_h$) position and Pitch, roll, yaw axes of rotation and a binary button located on the stylus. The outputs are three axes of force ($F_{h,x}\, F_{h,y}\, F_{h,z}$).

The axes of the haptic device ($X_h\, Y_h\, Z_h$) as shown in Figure 3.5 are set it to match the cantilever axes ($X_p\, Y_p\, Z_p$) as shown in Figure 3.2 for the cantilever. This is to make the user feel the same direction of force on the normal and lateral direction by using the haptic.

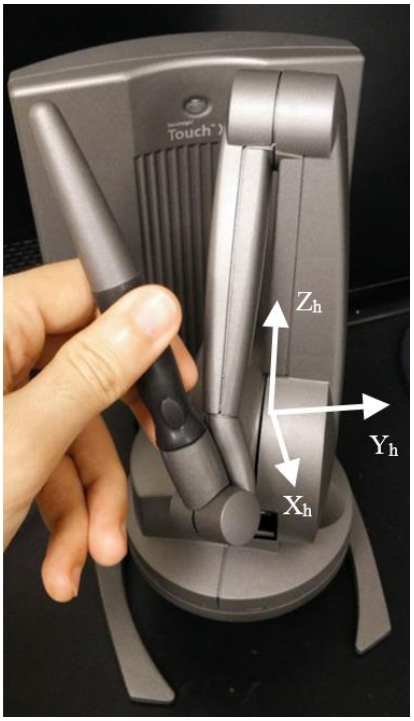

Figure 3.5 Photo of the Geomagic Touch X haptic device

The haptic comes with two Ethernet ports to connect the device with a PC. Using Ethernet cable to connect the device with a USB Ethernet Adapter as shown in Figure 3.6. This adapter has a USB port as an output to the host PC.

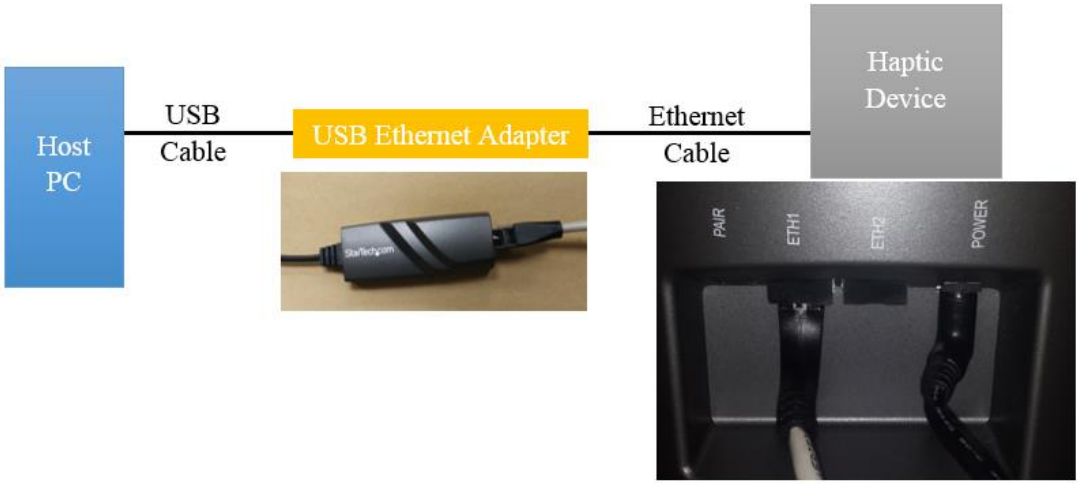

Figure 3.6 Haptic device to host PC connection

Figure 3.7 shows a block diagram for the AFM and the haptic device software and hardware. Starting from the right, the user changes the stylus position X_h, Y_h, Z_h of the haptic device to change the cantilever (probe) position X_p, Y_p, Z_p at the end. At each clock cycle of the haptic device, the stylus position is measured and transferred to the host PC. A separate clock on the PC is used to trigger the transfer of the stylus position to the Real-time system (target). When the target gets the haptic position, it scales the values to fit to the picocube range. At each clock cycle of the real-time system, the scaled values are applied as set point (reference position) for the PI controller of the PicoCube™. The PI control loop applies input voltages to the PicoCube™ to move the PicoCube™, and thus the probe, to the set point. Deflection of the cantilever probe is measured by real-time system from the photodetector voltages, V_n and V_l. The forces on the probe, F_n and F_l are calculated with (7) and (8). Haptic forces, scaled from F_n and F_l are calculated on the real-time system and transferred to the host at 0.1 ms clock cycle (real-time system communication clock), which is then transferred to the haptic device at each 2 ms clock cycle (haptic communication clock). Thus, the interconnection of the entire process allows the user to feel the force on the stylus, as the position of the haptic changes. Pressing the stylus button temporarily disables the force and position interaction.

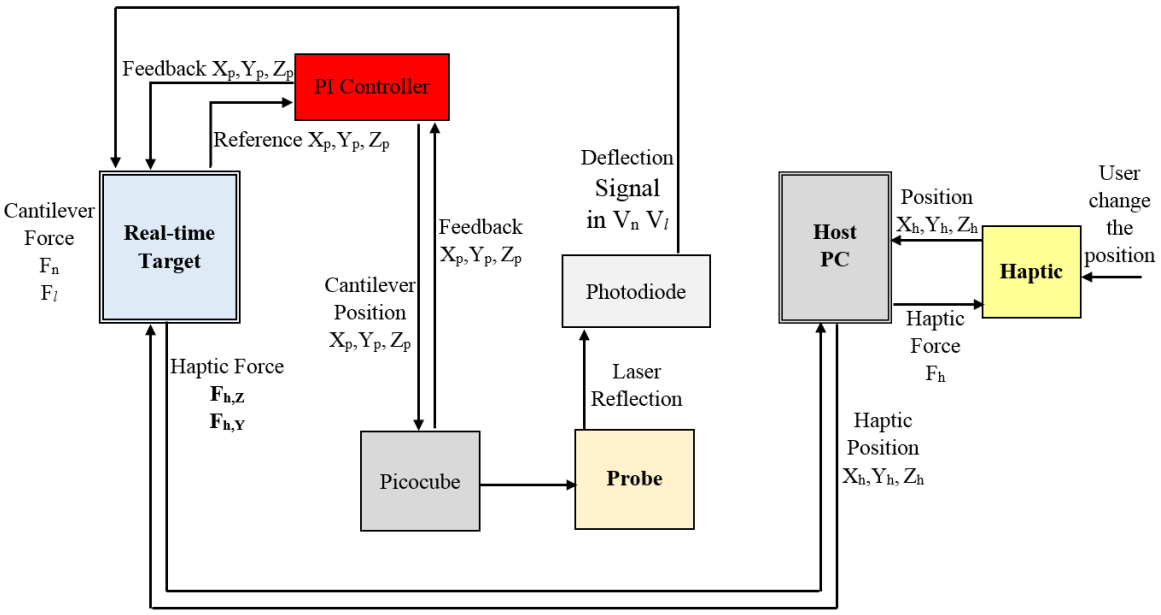

Figure 3.7 Block diagram of the AFM integrated with haptic device

$$F_{h,Z} = F_n K_f \tag{9}$$

$$F_{h,Y} = F_l K_f \tag{10}$$

where K_f is the scale between the cantilever force and the haptic in Z and Y axes. This gain is important to amplify the forces from the cantilever since the forces acted on the tip are very small (F_n and $F_l \approx$ nN).

3.3. SYSTEM SOFTWARE INTERACTION

There are three primary software pieces for using the AFM integrated with haptic device, each is coded separately. Software for interacting with the haptic device is written in the C\C++ programing language, and runs on the host PC. The microstages control software is written in LabView and runs on the host PC. The nanostages, picocube, and photodiode software control runs on the target PC using software written with LabVIEW Real-Time Module as shown in Figure 3.8.

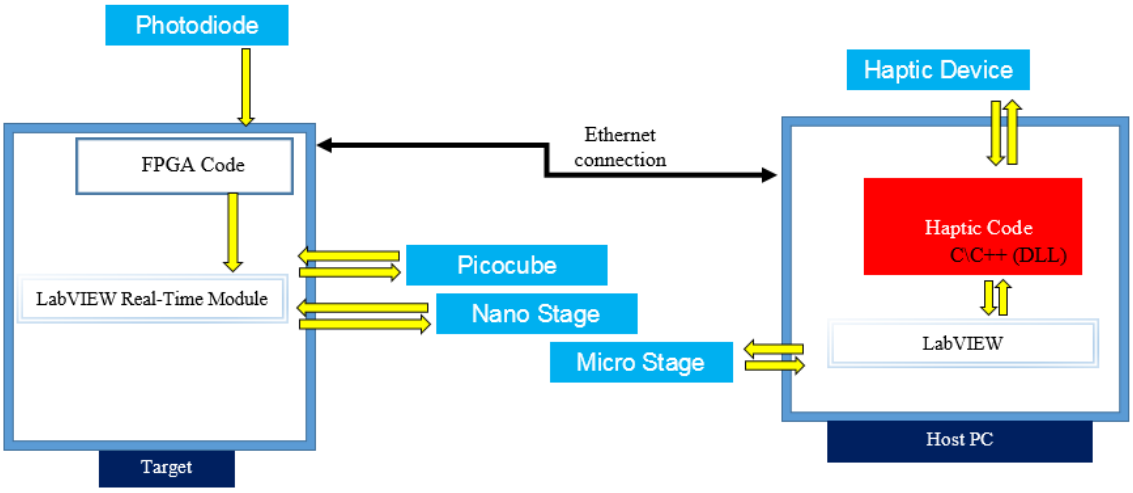

Figure 3.8 The AFM system software interaction

3.3.1. Haptic Device. The haptic device comes with a OpenHaptics Software Development toolKit (SDK) that includes the OpenHaptics Programmer's Guide and OpenHaptics API Reference. The OpenHaptics SDK is used to program the haptic device. As discussed above, the haptic device software is used to read position and write forces to the haptic. This toolkit provides Haptic Device API (HDAPI), and Haptic Library API (HLAPI) which contain examples and a library of C\C++ code for the haptic. From the

OpenHaptics Programmer's Guide "HDAPI requires the developer to manage direct force calculation for the haptic device whereas HLAPI handles the computations of haptic rendering based on geometric primitives, transforms, and material properties" [24].

Therefore, the HDAPI example and libraries where used to code the haptic. There are three methods to run the haptic from LabVIEW:

1) Import the entire functions of the HDAPI library using shared library then build the code.

2) Import one by one function from HDAPI library using call library function node.

3) Create what is needed in C\C++ and then build it into a dynamic-link library (DLL) that is imported to LabVIEW.

The third method is found to be the easier to use with less code complexity and less debugging needed, which is difficult to do since the code must be compiled an integrated into Labview and thus cannot be debugged in operation. So, once building the proper C\C++ code for the haptic, a dynamic-link library (DLL) is created to make the host PC through LabVIEW communicates with haptic. This DLL should follow a specific main steps, a flow chart of what the DLL main steps appear is shown in Figure 3.9.

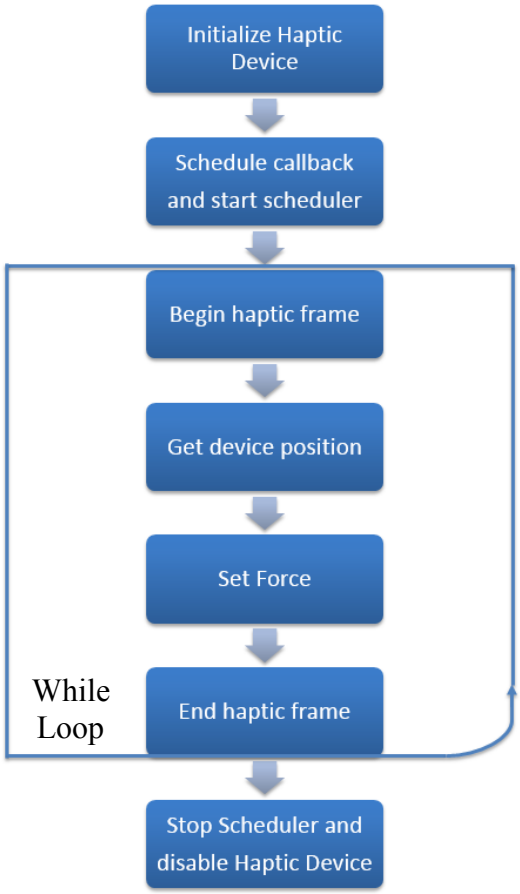

Figure 3.9 A flow chart of the main steps of a simple HDAPI program

Each step of the program flow chart shown in Figure 3.9 is done in sequence. The first step is to initialize the device and start the scheduler. The scheduler from the OpenHaptics Programmer's Guide is "manages a high frequency, high priority thread for sending forces and retrieving state information from the device"[24]. From beginning the haptic frame until ending the frame should be inside a while loop, where the haptic frame is the while loop shown in Figure 3.9 that calculates the forces for the device per each run. Thus, the haptic will send stylus position (X_h, Y_h, Z_h) and will receive the haptic force (F_h) only once per each loop run. Increasing the rate of the frame loop will provide more

stability and responsiveness of the device [25]. Note that increasing the rate will increase the amount of the central processing unit (CPU) being used in the host PC.

3.3.2. Host PC. The host PC runs a LabVIEW program which operates the user interface, interfaces with the real-time system, and operates the haptic device and the micro stage, as shown in Figure 3.8. The haptic's DLL functions are being called from LabVIEW in the host PC using Call Library Function Node (CLFN); this method is used to call a specific function on C\C++ DLL file. Function prototype in C/C++ code does not exactly match the style in LabVIEW, where the function prototype is the data type of the parameter that the function is using, Table 3.4 shows the different in data type of the parameters between C\C++ and LabVIEW. Since, some of the functions are not supported in LabVIEW [26]. Also, some of the data type needs to be changed to match the LabVIEW style as shown in table 3.4 [27][28].The frame loop of the haptic device as shown in Figure 3.9 is set to run at the haptic communication clock rate in the DLL and LabVIEW.

Table 3.4 Numeric parameters between C\C++ and LabVIEW [27][28]

Numeric Data Type Setting	Equivalent C Data Type
Signed 8-bit Integer	char
Signed 32-bit Integer	long
Unsigned 32-bit Integer	unsigned long
64-bit Real Number	double
Signed 32-bit Integer	integer

3.3.3. Real-time System. The real-time system runs the nano stage and picocube using LabVIEW Real-Time Module where the photodiode detector is running on the real-time system using a field programmable gate array (FPGA) and communicate with LabVIEW Real-Time Module as shown in Figure 3.8. The FPGA is used to measure and

process the photodiode signal, which requires a higher speed sampling and processing than is possible on the target (the FPGA runs at a 40 MHz rate whereas the LabVIEW Real-Time Module runs at 10 kHz).

Also, the LabVIEW Real-Time Module can move the micro stage by sending the new set point using network variable to the host PC. So, the user can control the position of the micro stage, nano stage, and picocube from the LabVIEW Real-Time Module interface which makes the system easier to use with one panel rather than using each part of the system separately.

3.4. ENGAGING THE CANTILEVER WITH SAMPLE

The user cannot engage the cantilever tip with surface of the sample using the haptic-picocube coupled motion. Therefore, an algorithm is needed to detect if the tip of the cantilever is engaged with the sample, and if not, guide the microstage and nanostage to engage the tip. Before moving the picocube or the nano stage to bring the cantilever and the sample closer to one other using jogs or the engage algorithm, it is important to smooth the step input to avoid damaging the expensive piezoelectric stages. Therefore, a smooth interpolator such as the Linear Segments with Parabolic Blends interpolator (LSPD) is needed to perform this step [30].

In this thesis, a contact mode is used as method of contact between the cantilever and the surface. Therefore, if a certain change in the photodiode vertical signal with a small change in the picocube position, this means a contact occurred between the sample and the tip of the cantilever; bending on the cantilever happened.

The flow chart in Figure 3.10 shows the engage process that was developed. Before running the algorithm it is better to make the sample as close as possible using the human eye and moving the sample using the micro stage for faster movement until the sample is close to the probe. Next, using the algorithm in Figure 3.10, the procedure starts with checking the set point of the photodiode vertical signal if it is reached or not. If not, the nano stage will move up a small step with 1 nm increment. If he nano stage reached maximum position which 0.2 µm, then the nano stage will go down to 0 µm position. Once the nano stage reached the 0 µm position the micro stage starts moving up with 0.16 µm increment which is 80% from the nano stage range. This process will continue until the photodiode vertical signal starts to change and reached the set point which means the tip of the cantilever touched the sample surface.

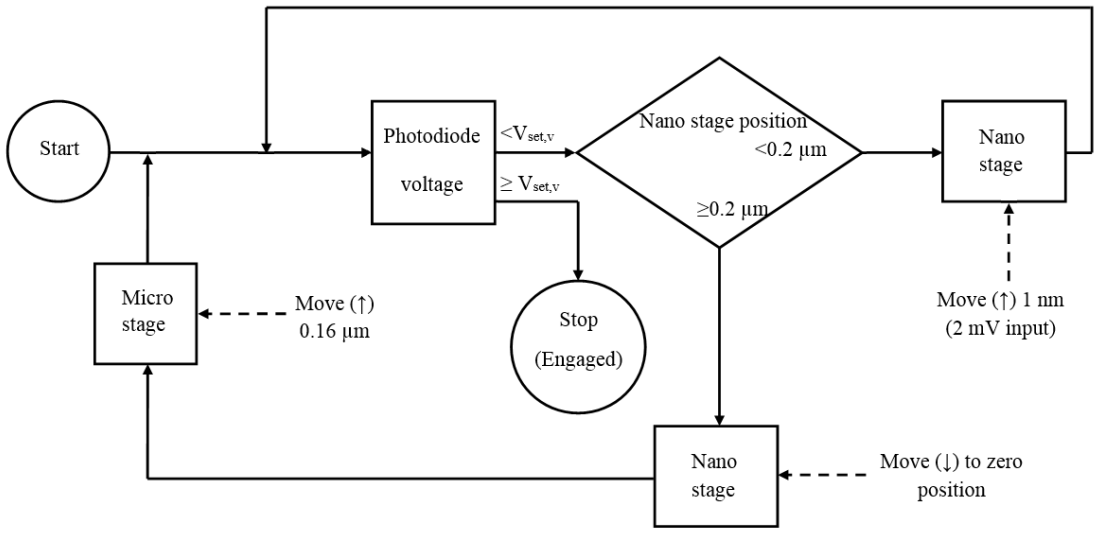

Figure 3.10 Engaging the cantilever with sample process flow chart

This method also can be used with replacing the nano stage movement by the picocube. The picocube is better to use if the haptic-picocube coupled motion will be used. However the nano stage movement is important for the future work especially for the dual -probe atomic force microscopy.

4. EXPERIMENTAL RESULTS AND ANALYSIS

Haptic testing, calibration, and filter design for noise reduction in the haptic interface are presented in this section. Rectangular and triangular cantilevers type is used to perform the experiment and test the forces impacting these type of cantilevers. The system is calibrated by adjusting the forces (i.e., normal and lateral) to improve the fidelity of the system (Section 4.1) [10]. Furthermore, the relationship between the sensitivity of the haptic-picocube position with the resolution and range of the picocube are clarified. In addition, the haptic force sensitivity with the photodiode output is explained (Section 4.2). In this chapter, a low-pass filter is used for the photodiode signal to remove high-frequency noise from the signal (Section 4.3).

A contact mode rectangular cantilever (Top Visual Contact Silicon Cantilevers VIT_P_C-A series [29]) is used to obtain most of the results in this chapter. The cantilever used is show in Figure 4.1. The specifications of this cantilever are presented in Table 4.1.

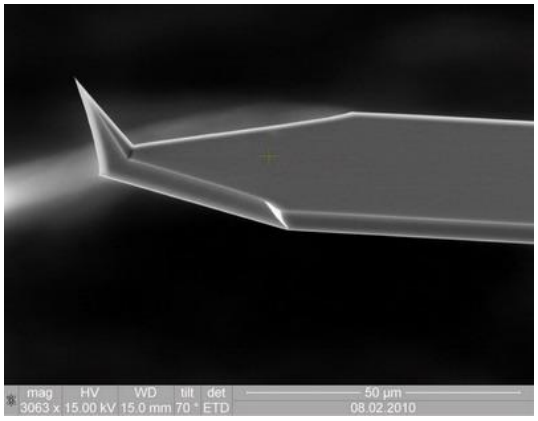

Figure 4.1 Photo of Top Visual Contact Silicon Cantilevers VIT_P_C-A series [29]

After placing the probe on the picocube holder, the holder is then placed on the picocube to point the laser at the end of the cantilever to obtain the best sensitivity and least noise from the photodiode output signal. Figure 4.2 provides an image of the probe on the picocube holder and Figure 4.3 shows the picocube holder positioned with the cantilever positioned above the picocube.

Table 4.1 Cantilever specification [29]

Cantilever length, L	450 µm
Cantilever width, W	50 µm
Cantilever thickness, t	2.5 µm
Tip height, h	15 µm
Force constant, k	0.3 N/m

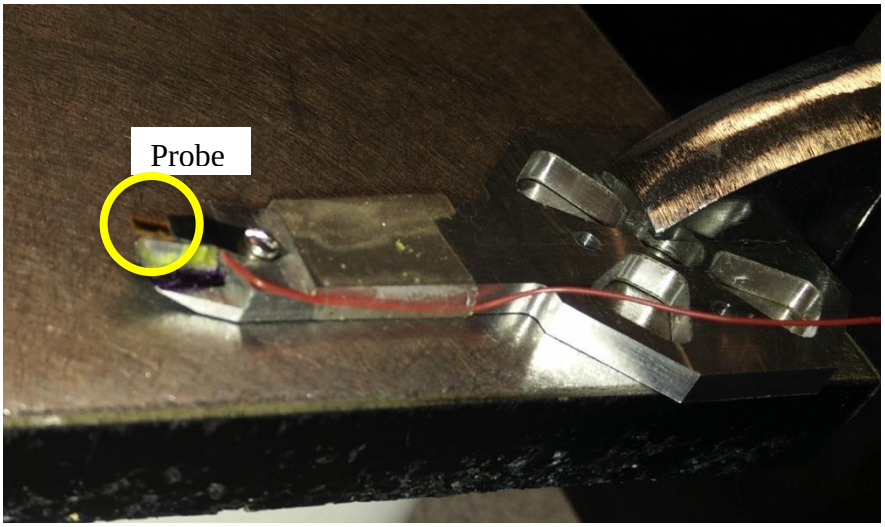

Figure 4.2 Contact mode cantilever placed on the picocube holder

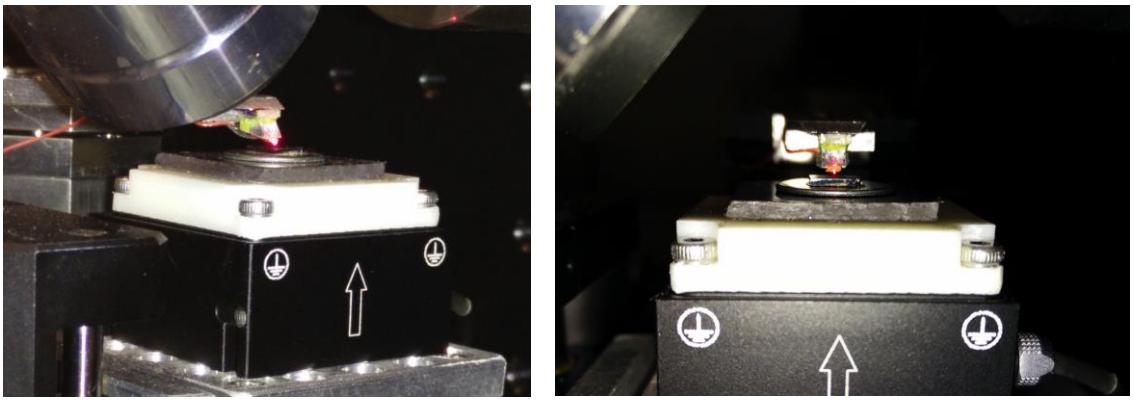

(a) (b)

Figure 4.3 The picocube holder with the cantilever is placed above the sample, and a laser pointed on the cantilever end. (a) Perspective view (b) Side view

Using a spot at the end of the cantilever is important to avoid noise from the photodiode signal output. Figure 4.4 shows the effect of using reflection on the cantilever as well as the differences between the use of a triangular cantilever and a rectangular cantilever. In addition, Figure 4.5 shows the fast Fourier transform (FFT) of both signals.

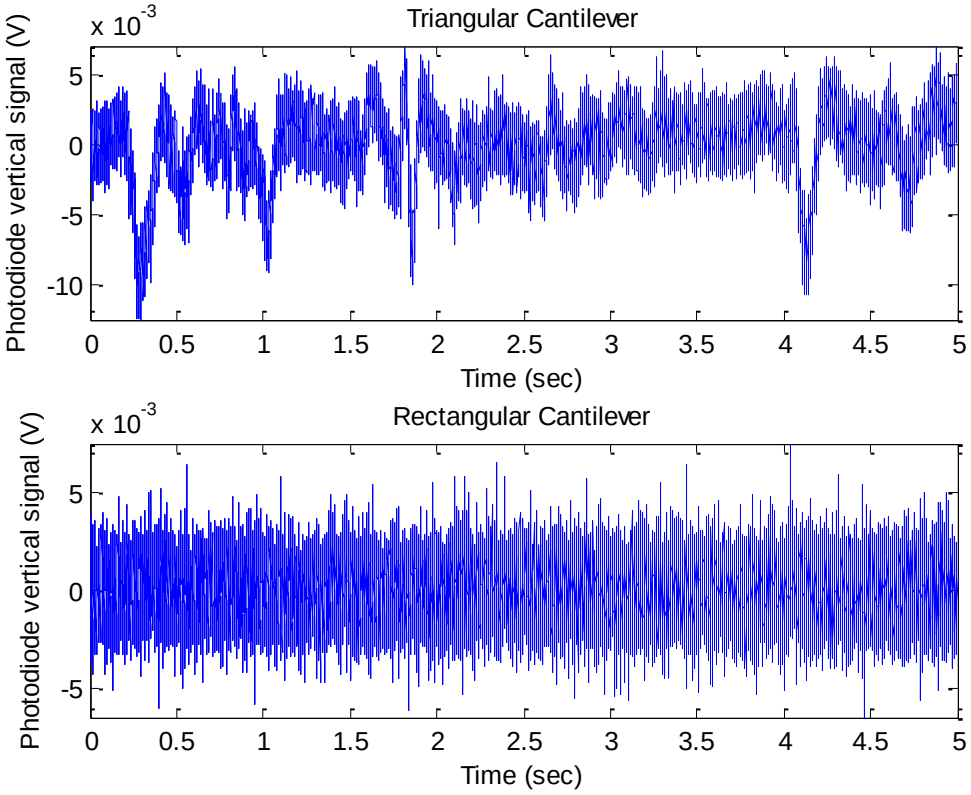

Figure 4.4 The photodiode vertical voltage signal in disengaged case for 5 seconds

When sending the sample away from the cantilever, the difference in maximum and minimum values for the triangular cantilever is 0.0195 V and 0.0140 V for the rectangular cantilever. The triangular cantilever showed some low frequency noise between 0 to 60 Hz, on the contrary, the rectangular cantilever showed less low frequency noise at the same range.

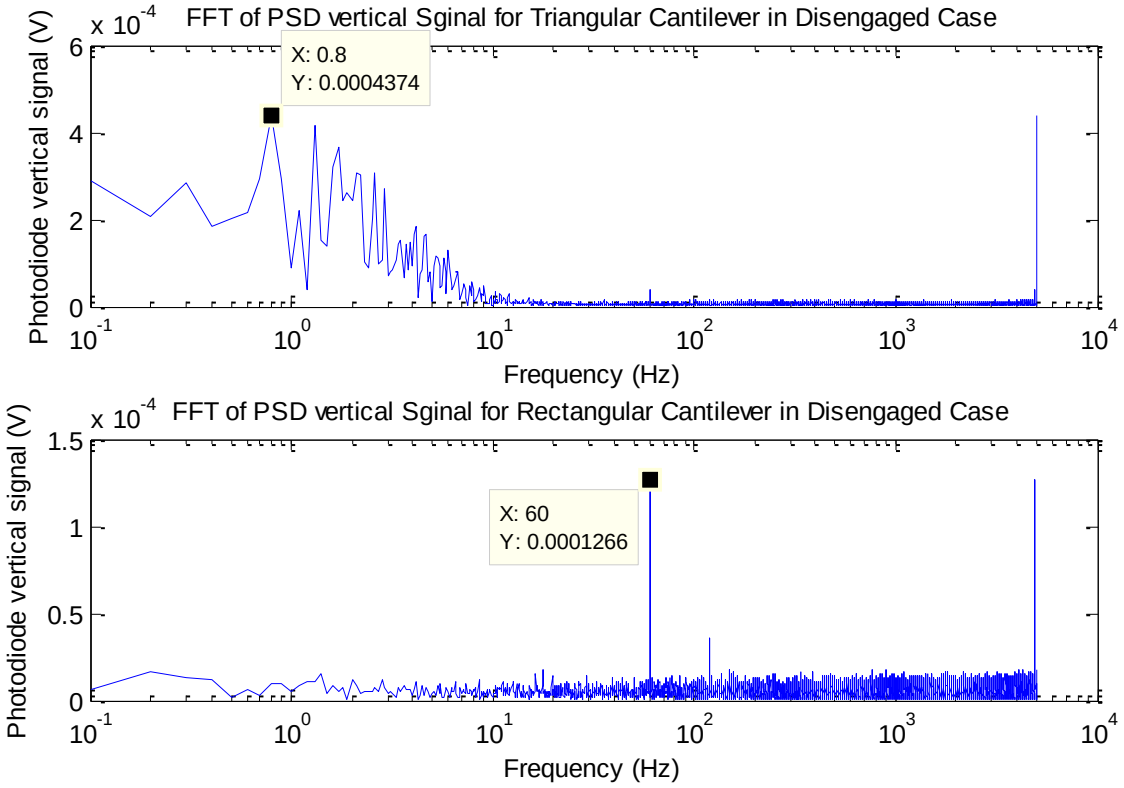

Figure 4.5 The FFT of the photodiode vertical voltage signal in disengaged case for 5 seconds

Figure 4.6 shows an example of moving the picocube with an LSPD interpolator for the 1000 nm step input to the interpolator before engaging the probe with the sample.

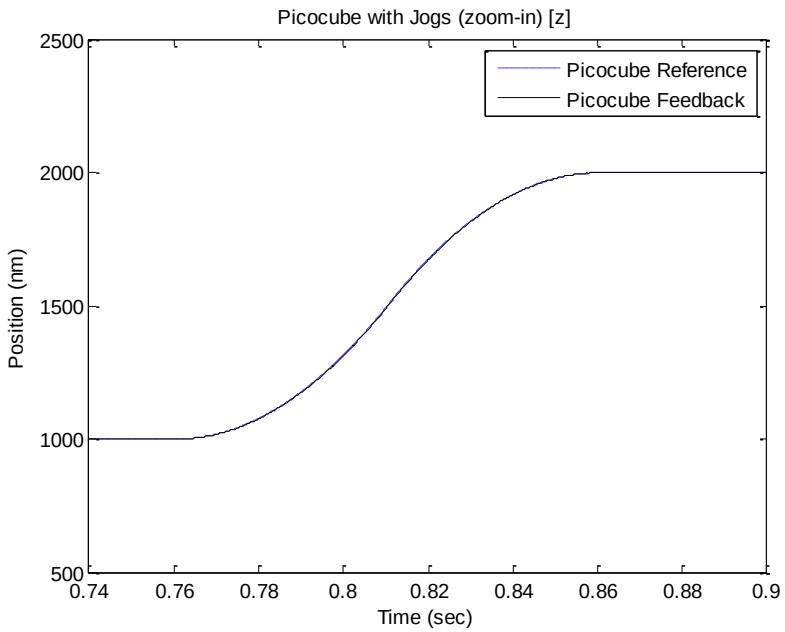

Figure 4.6 Picocube motion using LSPD interpolator with 1000 nm step input for Z-direction

4.1. FORCE CALIBRATION

It is important to calibrate the forces on the tip precisely to ensure that the forces that act on the haptic and the cantilever are accurate. Thus, the normal (S_n) and lateral (G_l) gains are calibrated for the haptic-AFM system using the rectangular cantilever. Section 4.1.1 explains the method of calibrating the normal gain while Section 4.1.2 explains the method of calibrating the lateral gain for the system.

4.1.1. Normal Gain Calibration. Signal gain in the normal direction or sensitivity of the optical device (S_n) is obtained from the slope between the photodiode vertical signal and picocube Z-axis position. First, the XY movement of the picocube is fixed to find this gain. Second, the cantilever is moved in the Z direction while the tip is touching the surface of the sample. Third, the picocube position (P_z in nm) is plotted with the photodiode vertical signal (V_v in V) as shown in Figure 4.7. This procedure is to eliminate any forces in XY

directions, and find the relation between the photodiode vertical signal and the cantilever position in Z direction only as shown in Figure 4.8.

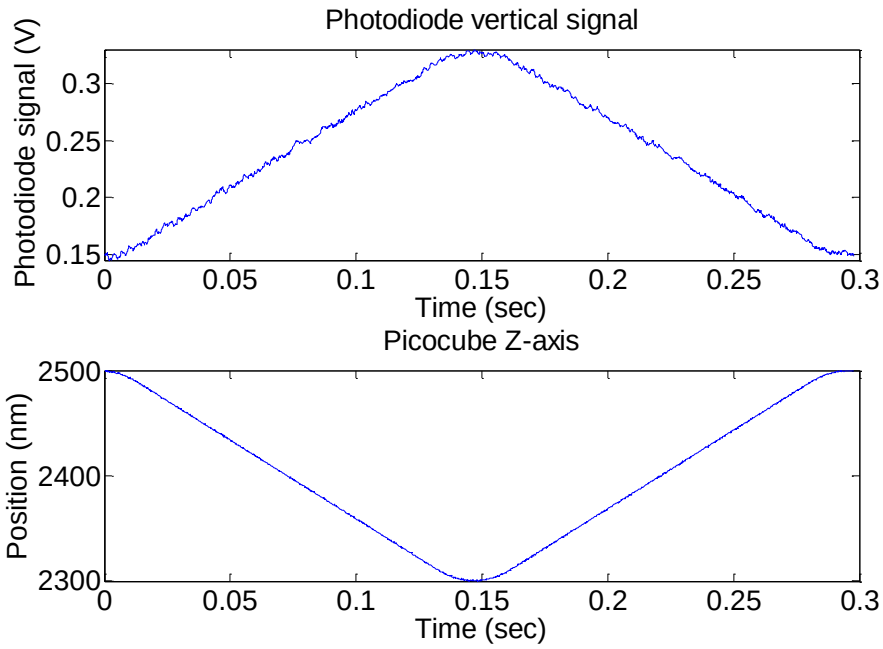

Figure 4.7 The photodiode vertical voltage signal and picocube Z-axis position in approach-retract case for 0.3 seconds

The signal gain in the normal direction (S_n in nm/V) is defined as,

$$S_n = \frac{dP_z}{dV_v} \tag{11}$$

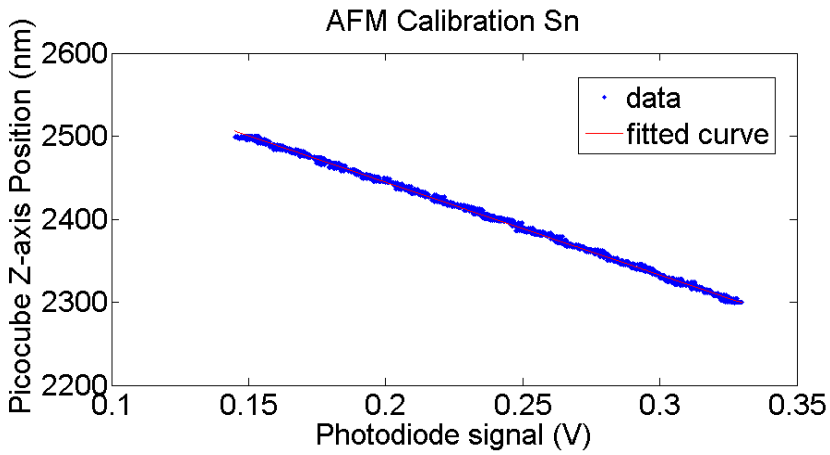

Figure 4.8 The photodiode vertical voltage signal and picocube Z-axis position in approach case only for 0.05 seconds

Based on Figure 4.8 using the linear polynomial curve, the line equation is,

$$V_v = S_n \cdot P_z + x \tag{12}$$

coefficient S_n (with 95% confidence bounds) is found to be 1117 nm/V. Also, with using the rectangular cantilever the normal cantilever stiffness (k) is 0.3 N/m, so, the normal force F_n in N in (7) is equal to,

$$F_n = 0.3 \cdot 10^{-9}\ V_v\ (-1117) \tag{13}$$

$$F_n = -335.1 \cdot 10^{-9}\ V_v \tag{14}$$

4.1.2. Lateral Gain Calibration. The lateral force on the cantilever is defined in equation (8). It is difficult to obtain S_l separately. However, finding ($G_l = k_l S_l / h$) is easier [10]. This section explains how to use this method to calibrate the lateral direction with respect to the normal direction. When a tilted sample is used, the cantilever is slid up and down, and the slope of the sample is known as shown in Figure 4.9. The force generated on the tip is,

$$F_n = N\cos\theta + (\mu N + A)\sin\theta \quad (15)$$

$$F_l = N\sin\theta + (\mu N + A)\cos\theta \quad (16)$$

$$F_n' = N'\cos\theta + (\mu N' + A)\sin\theta \quad (17)$$

$$F_l' = N'\sin\theta + (\mu N' + A)\cos\theta \quad (18)$$

where F_n and F_l are the normal and lateral forces, respectively, on the cantilever when sliding down. F_n' and F_l' are the normal and lateral forces, respectively, on the cantilever when sliding up, N is the repulsive force, and μN+A=f is the friction force from normal force and the adhesive force A. The angle of the tilted surface is θ.

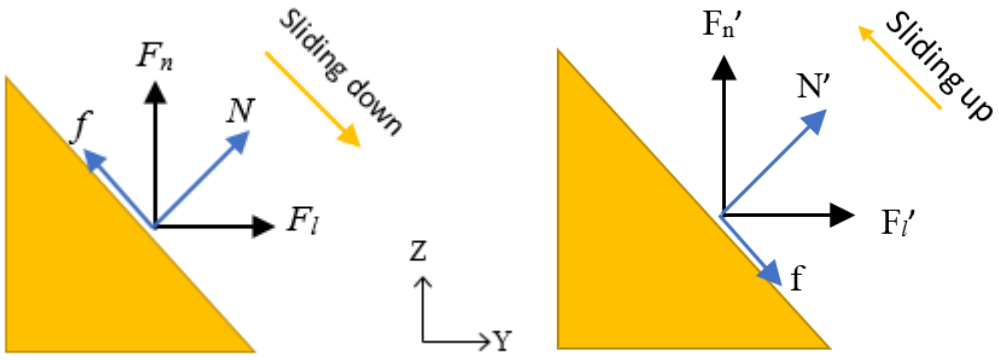

Figure 4.9 Forces components on the cantilever from sliding the tip on a tilted surface sample

The slope of the sample is calculated from imaging the sample surface as shown in Figure 4.10. The slope of the sample is not a perfect line (blue) so a line was generated (red) to fit the slope of the sample.

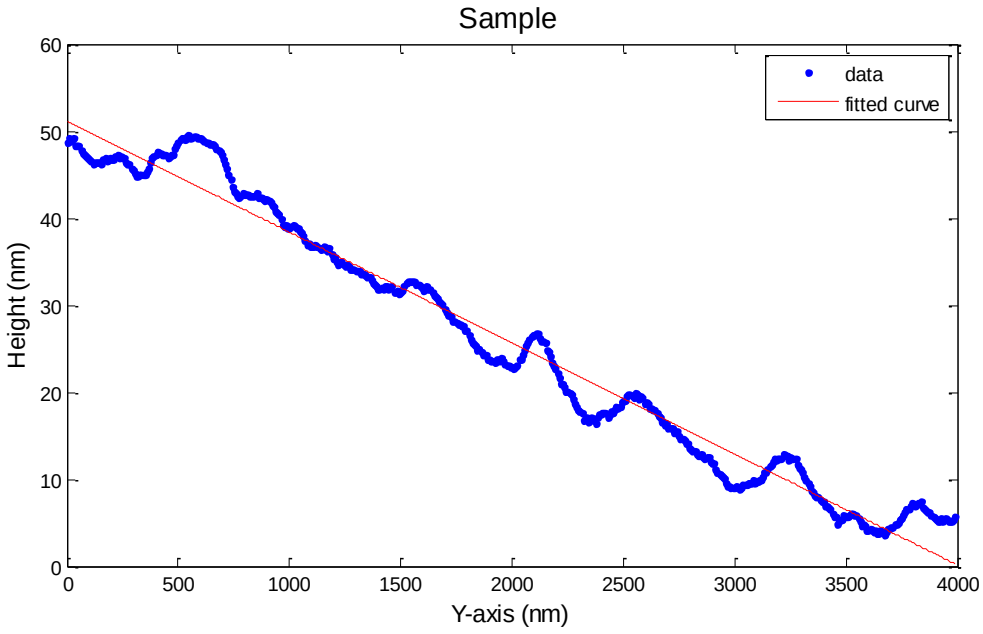

Figure 4.10 The surface slope of the sample from imaging mode (calibration sample)

Then,

$$\frac{\partial F_l}{\partial F_n} = \frac{\sin\theta + \mu\cos\theta}{\cos\theta - \mu\sin\theta} \tag{19}$$

$$\frac{\partial F_l'}{\partial F_n'} = \frac{\sin\theta - \mu\cos\theta}{\cos\theta + \mu\sin\theta} \tag{20}$$

And, from (7),

$$\frac{\partial V_v}{\partial F_n} = \frac{1}{kS_n} \tag{21}$$

Also, (8),

$$\frac{\partial F_l}{\partial V_h} = \frac{k_l S_l}{h} = G_l \tag{22}$$

Using equation (19) and (20) with (21) and (22), yields,

$$G_l \frac{\partial V_v}{\partial V_h} \frac{1}{kS_n} = \frac{\sin\theta - \mu\cos\theta}{\cos\theta + \mu\sin\theta} \tag{23}$$

$$G_l \frac{\partial V_v'}{\partial V_h} \frac{1}{kS_n} = \frac{\sin\theta + \mu\cos\theta}{\cos\theta - \mu\sin\theta} \tag{24}$$

To find the unknown (G_l and μ) in (23) and (24), the tip of the cantilever is slid along the Y-axis on the sample as shown in Figures 4.9 and 4.10 with zero change in the X-axis position. Performing these steps eliminates the force in the X direction. The result of moving the cantilever is shown in Figure 4.11.

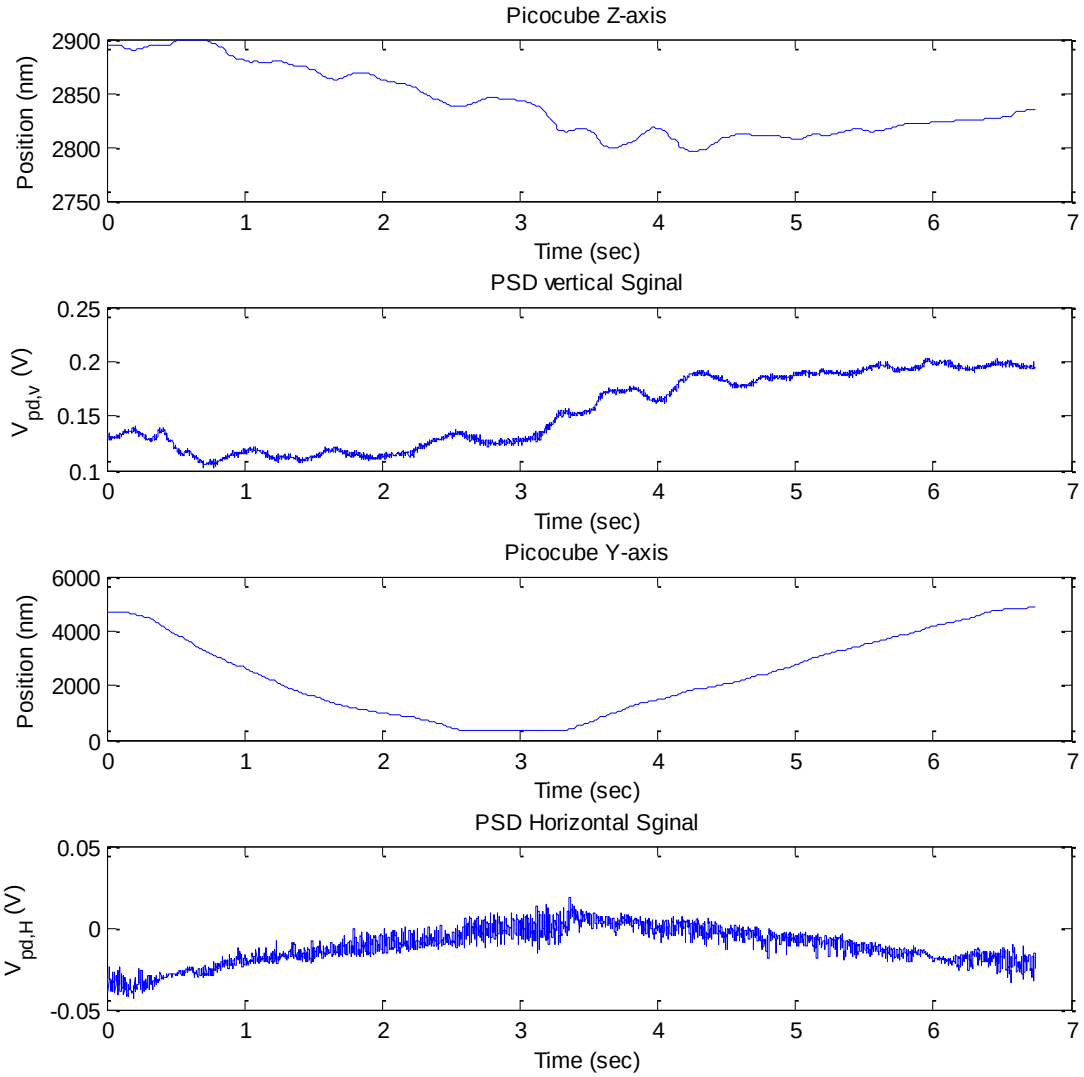

Figure 4.11 The photodiode signal in vertical and horizontal direction in V with moving the picocube in Z and Y axes in nm for 7 seconds

The result in Figure 4.12 is from sliding the cantilever down as shown in Figure 4.9 on the sample in YZ plane to obtain $\frac{\partial V_v}{\partial V_h}$ in (23).

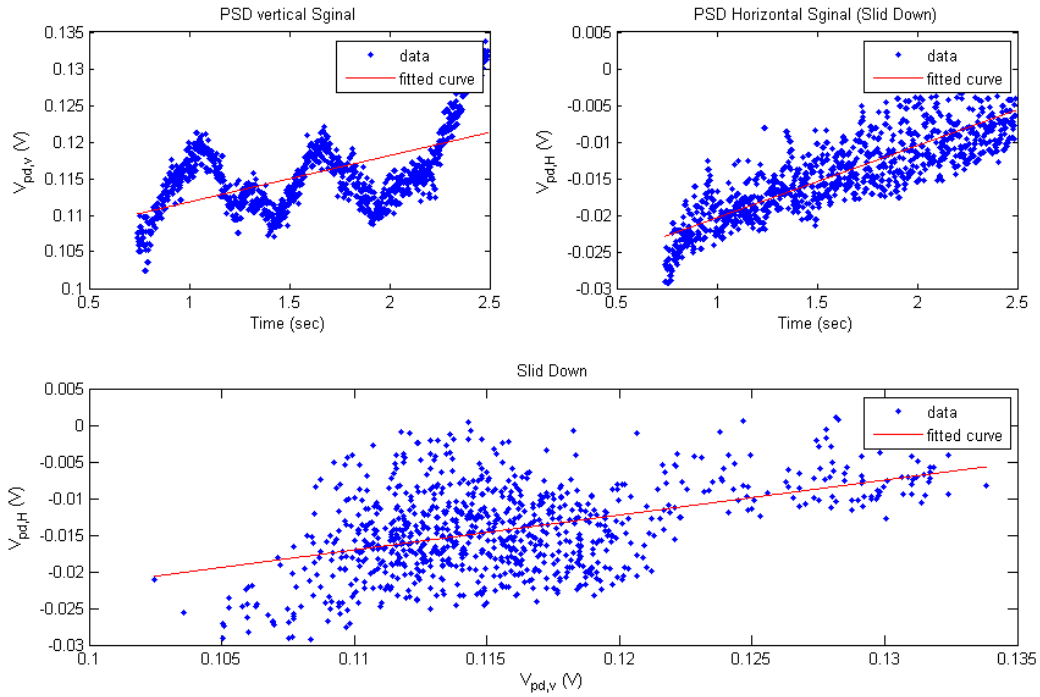

Figure 4.12 The vertical and horizontal photodiode signal in V from sliding the cantilever down on the sample

The result in Figure 4.13 is from sliding the cantilever up as shown in Figure 4.9 on the sample in YZ plane to obtain $\frac{\partial V_v'}{\partial V_h}$ in (24).

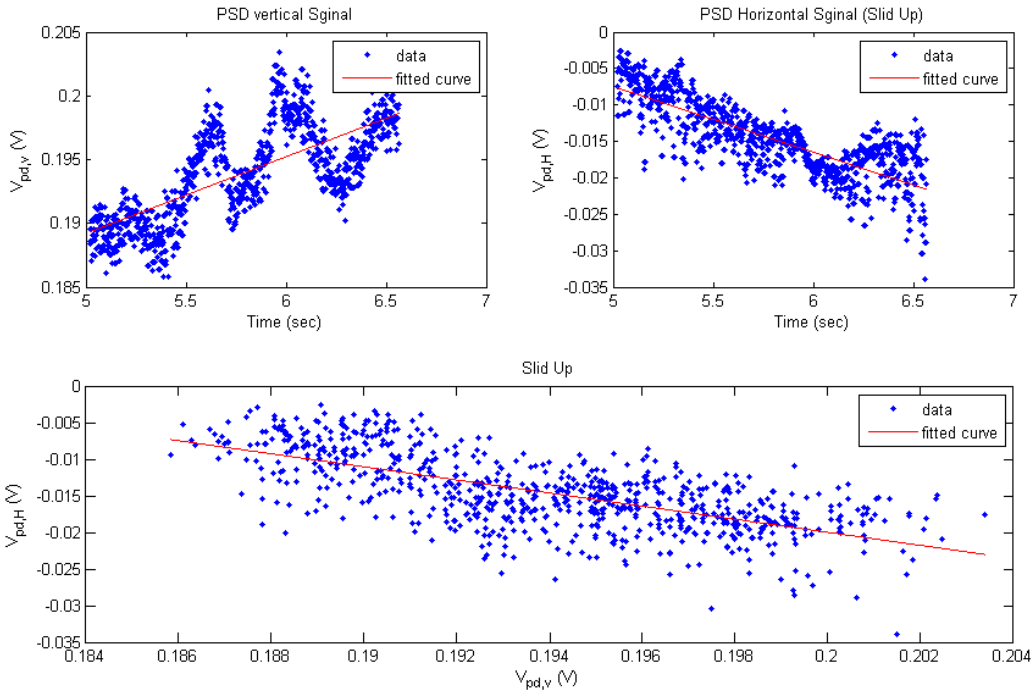

Figure 4.13 The vertical and horizontal photodiode signal in V from sliding the cantilever up on the sample

To find G_l and μ, the nonlinear (20) and (21) are solved using the graphical method as shown in Figure 4.14. The result from the graphical solution is G_l = -63.78 nN/V which turns (8) into

$$F_l = -63.78 \cdot 10^{-9} V_h \tag{25}$$

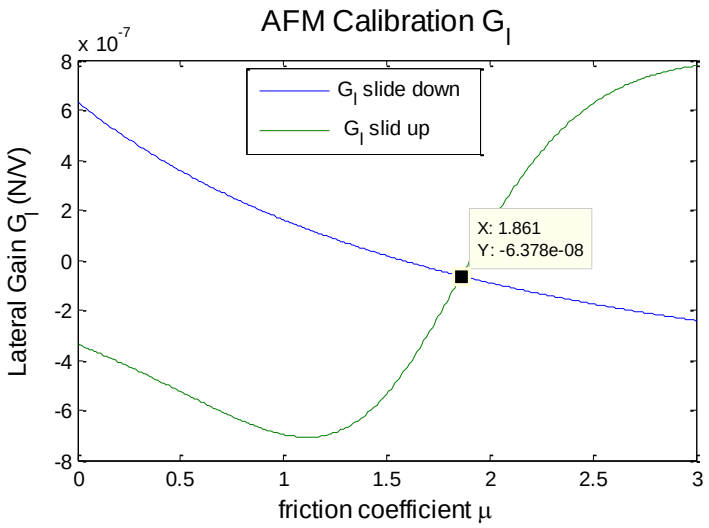

Figure 4.14 The solution of ($G_l = k_l S_l / h$) from equation (20) and (21). μ=1.861, and G_l =-63.78 nN/V

4.2. FORCE AND POSITION VS. RANGE SCALING

It is important to know the range of motion of the haptic and the picocube, also the sensitivity of the haptic-picocube coupled motion to perform any cantilever displacement above the sample surface. In addition, it is important for the user to know the haptic force in terms of the cantilever deflection. Section 4.2.1 explains the relationship between the motion of the haptic and picocube, resolution, and range of the picocube. Section 4.2.2 clarifies the relationship between the haptic forces and the cantilever's vertical and horizontal displacements.

4.2.1. Haptic-picocube Resolution. At different times in operation, the user will need to be able to move the probe over long ranges, for instance when locating certain features. At other times, the user will require very precise motion, as in manipulation tasks. The sensitivity setting, or conversion from mm in haptic motion to nm in picocube motion, can be used to select the tradeoff between range of motion and precision of motion. Because of the limited measurement sensitivity and range of the haptic, it is not possible to have

high resolution, precise motion at the same time and long range motion. The measurement sensitivity of the haptic is 0.023 mm, however the human's hand sensitivity is about 1 mm. Therefore, the user should be aware of the range of picocube motion and resolution in nm with respect to the range of the haptic and the human's hand sensitivity. The maximum range for the picocube is 5000 nm and the minimum resolution is 0.1 nm. The 120 mm range of motion for X and Z axes and the 160 mm for Y axis of the haptic device are used for all experiments. Table 4.2 and Table 4.3 show the important relationship between the sensitivity of the haptic-picocube coupled motion with the resolution and range of the picocube in nm for X and Z axes and Y axis, respectively.

Table 4.2 Haptic-picocube sensitivity, resolution, and range of picocube for X and Z axes

Sensitivity (pico nm/haptic mm)	Resolution (pico nm)	Range (pico nm)
5000/120	41.7	5000
1200/120	10	1200
1000/120	8.3	1000
500/120	4.2	500
120/120	1	120
100/120	0.8	100
12/120	0.1	12

Table 4.3 Haptic-picocube sensitivity, resolution, and range of picocube for Y axis

Sensitivity (pico nm/haptic mm)	Resolution (pico nm)	Range (pico nm)
5000/160	31.3	5000
1600/160	10	1600
1000/160	6.3	1000
500/160	3.1	500
160/160	1	160
100/160	0.6	100
16/160	0.1	16

4.2.2. Force Sensitivity. The user will need to be able to identify a certain features from moving the probe over sample, so, the user will require very precise force feedback to the haptic, as in manipulation tasks. The force sensitivity, or conversion from nN in the probe to N in haptic, can be used to show the relation between probe displacement and haptic force. Because of the limited probe displacement and force on the user hand from the haptic, it is not possible to have high force, precise motion at the same time. Making the conversion very small will create an environment where the user will not notice small changes in the probe force. When using a large conversion, the user will undergo a huge force that prevents the user from moving the probe in a smooth and effortless manner.

The normal and lateral forces are defined in equations (7) and (8), respectively. The force applied on the haptic according to the forces on the cantilever are stated in equations (9) and (10). The K_f gain amplifies the nN force from the probe into an N to allow the user to feel the forces from the haptic. Experiments have found that the value of K_f is 15×10^6. This value is suitable for the user to feel the force compared with the range of motion between the picocube and the probe deflection. A normal (Z axis force) range between 0.5 to 3 N is comfortable and suitable for the user to feel using the haptic. The force sensitivity

for the chosen K_f between the photodiode voltage output as an input and the force applied to the haptic as an output are shown in Table 4.4. The photodiode signal output has a minimum value equal to -1 V and a maximum value equal to 1 V as calculated from equations (3) and (5).

Table 4.4 Force sensitivity

Output/Input	(N/V)
$F_{h,z}/V_v$	5.0265
$F_{h,y}/V_h$	0.9567

The relation between the vertical displacement (δ_z) of the probe and the haptic force in Z direction is found from (4) and (9), therefore,

$$\frac{F_{h,Z}}{\delta_z} = \frac{K_f F_n}{S_n V_v} = \frac{K_f k S_n V_v}{S_n V_v} = K_f k \tag{26}$$

Table 4.5 shows the relation of haptic force on the Z axis with respect to the probe vertical displacement.

Table 4.5 Haptic Z axis force with respect to the probe vertical displacement

δ_z (nm)	$F_{h,z}$ (N)
0	0
100	0.45
200	0.9
500	2.25
700	3.38
1000	4.5

On the other hand, the relation between the horizontal displacement (δ_y) of the probe and the haptic force in Y direction is found from (6) and (10), therefore,

$$\frac{F_{h,Y}}{\delta_y} = \frac{K_f F_l}{hS_l V_h} = \frac{K_f k_l S_l V_h}{h^2 S_l V_h} = \frac{K_f k_l}{h^2} \tag{27}$$

Since k_l is very hard to find by itself and the angle of twist θ_x is small, so the sensetivty can be estimated as $S_l \approx S_n/l$, therefore (27) can be estimated as [10],

$$\frac{F_{h,Y}}{\delta_y} \approx \frac{K_f G_l V_h}{h\frac{S_n}{l} V_h} = \frac{K_f G_l l}{hS_n} \tag{28}$$

Table 4.6 shows the range of haptic forces on the Y axis with respect to the probe horizontal displacement.

Table 4.6 Haptic Y axis force with respect to the probe horizontal displacement

δ_y (nm)	θ_x (deg)	$F_{h,y}$ (N)
0	0	0
10	0.04	0.26
25	0.10	0.64
50	0.19	1.28
100	0.38	2.57
150	0.57	3.85

4.3. NOISE AND FILTER DESIGN

In addition to cantilever deflection, noise in the photodiode measurement is transmitted to the haptic device. Large noise can overwhelm the cantilever deflection signal, making it difficult for the user to feel subtle changes in force. When the noise is sufficiently large (and the user's grip sufficiently compliant), the noise-induced forces can create motion on the haptic device. The haptic device motion then causes undesirable motion in the probe. This undesirable feedback cannot be stopped, but it can be mitigated

by removing as some of the noise transmitted to the haptic through filtering the photodiode signal.

The maximum frequency of the human response is approximately 10 Hz as a maximum frequency response [32]. Therefore, the user's hand cannot move the haptic stylus more than this rate. An experiment is done to prove this human hand bandwidth. The experiment is setup by making the user to hold the stylus while a sinusoid force (F) in N is applied on the haptic, F is defined as,

$$F(t) = A\sin(2\pi f\ t) \tag{29}$$

where A is the amplitude, f is the frequency in Hz, and t is the time in second. The amplitude of the force for this experiment is fixed at 0.5 N, which suitable for the user in this experiment.

Figure 4.15 and Figure 4.16 show the result from applying the sinusoid force for f equal to 0.5, 10, 20, and 100 Hz. The result shows how the position frequency follows the frequency of the applied force. It is clear that the position follows the force input for f equal to 0.5 Hz. In the second chart of Figure 4.15, the position of the stylus is partially following the applied force. However, when the frequency of the force exceed the 10 Hz, it is hard to recognize the frequency of the applied force from the output position as shown in third chart (f = 20 Hz). The higher the frequency of the force (output) then the lower this will affect the position (output) of the haptic as shown in the fourth chart (f = 100 Hz).

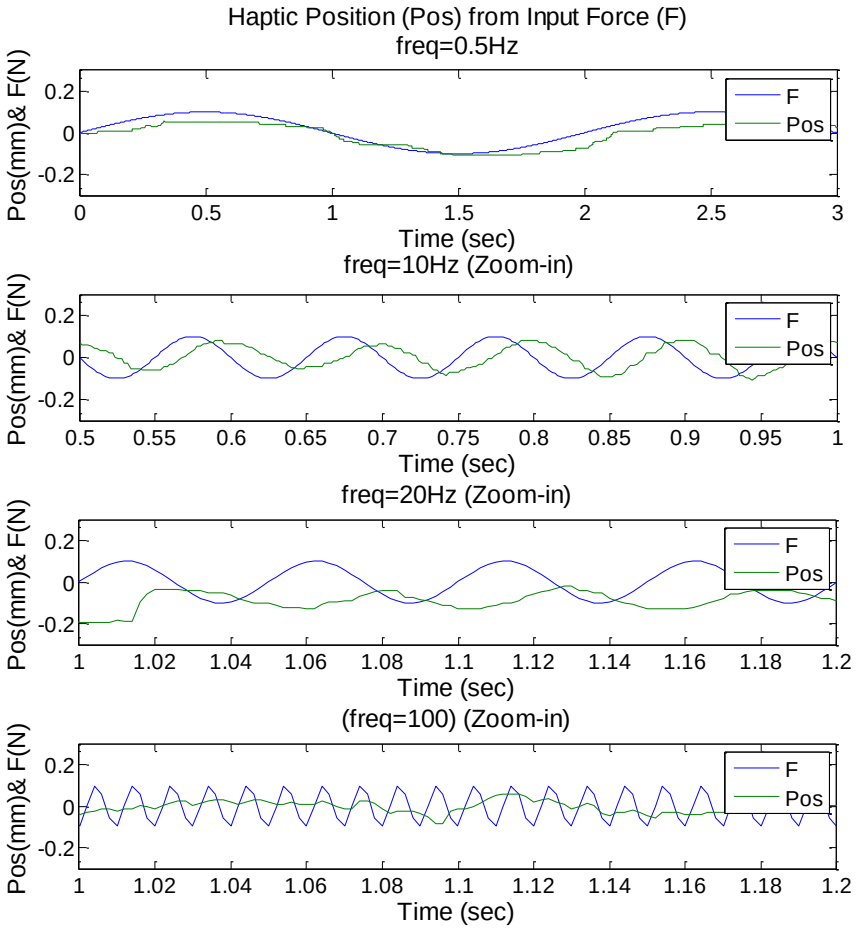

Figure 4.15 Haptic position for different force's frequencies applied (freq=0.5, 10, 20, and 100 Hz)

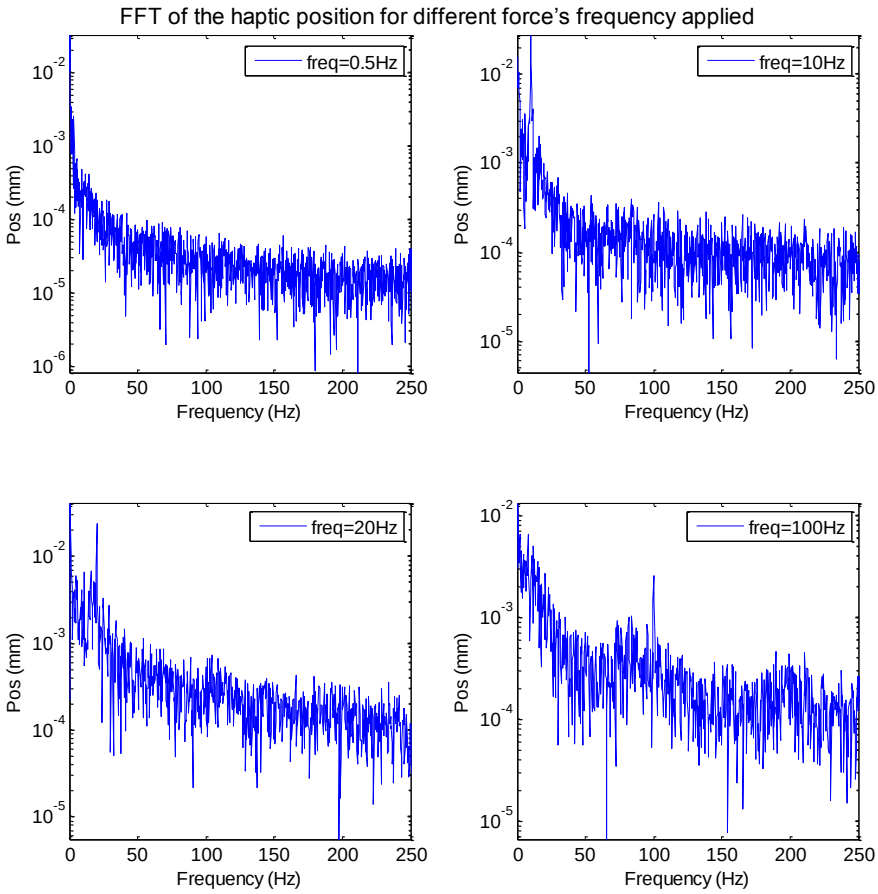

Figure 4.16 FFT of the haptic position for different force's frequencies applied (freq=0.5, 10, 20, and 100 Hz)

The FFT of the position of the haptic in Figure 4.15 is shown in Figure 4.16. The results shows that the effect of the force decreased if the force frequency increased. Moreover, at the second chart the maximum magnitude is at the same frequency applied (f = 10 Hz). However, at the third chart the maximum is not at the frequency applied (f = 20 Hz). Similarly for the fourth chart, it is clear that the effect of magnitude at the force's frequency is decreased (at 100 Hz it is 19% of the maximum magnitude).

Figure 4.17 shows the haptic model fitting using the frequency response. The fitted model has the transfer function H(s) as,

$$H(s) = \frac{K\omega_n^{\ 2}}{s^2 + 2\zeta\omega_n s + \omega_n^{\ 2}} = \frac{300}{s^2 + 100s + 10000} \tag{30}$$

where K is the gain that raises and lowers the magnitude, ω_n is the natural frequency in rad/sec, and ζ is the damping factor which affects the sharpness of the peak.

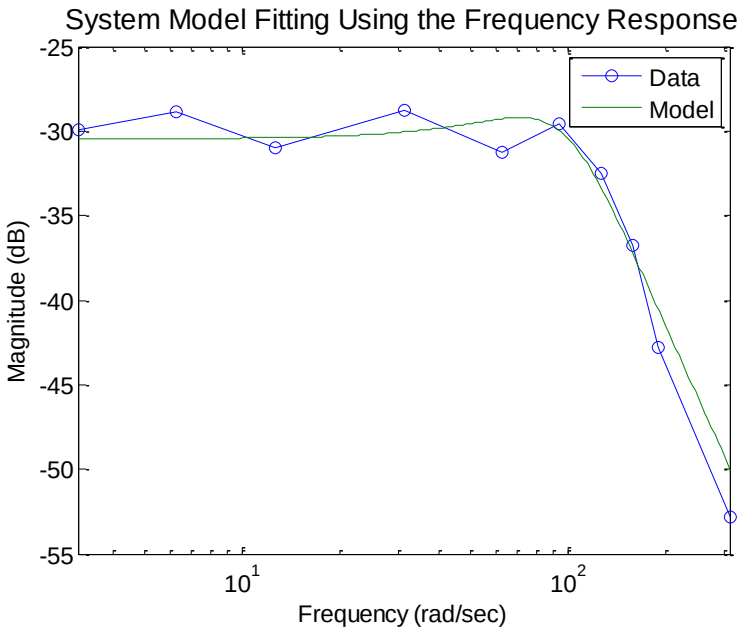

Figure 4.17 Haptic model fitting using the frequency response

Therefore, the forces that has frequency less than 16 Hz will affect the system as it is fed back to the probe position. However, the high frequency content will still affects the system as shown in Figure 4.18 and Figure 4.19. Therefore, a low pass filter should be used to remove this undesirable high frequency content from the input force to the haptic.

The photodiode signal is sampled at 40 MHz while the real time system is running at 10 kHz. Calculating the force from the real-time photodiode signal that is causing a high frequency noise on the haptic when the haptic-picocube coupled motion is used. Therefore, a low-pass filter is needed to eliminate this noise. The cutoff frequency ω_c should be less than the Nyquist frequency of the real time system rate which makes f_c equal to 5 kHz. The transfer function of low pass filter is defined as,

$$\frac{Y(s)}{X(s)} = \frac{\omega_c}{s + \omega_c} \tag{31}$$

where the X(s) is the input signal in s domain to the low pass filter and Y(s) is the output from the filter. The invers Laplace of equation (29) is,

$$\dot{y}(t) + \omega_c y(t) = \omega_c x(t) \tag{32}$$

The first-order backward difference discrete time approximation of the filter is,

$$\frac{y[k+1] - y[k]}{\Delta T} + \omega_c y[k] = \omega_c x[k] \tag{33}$$

where ΔT is the sampling period and k is the index =1, 2, …, N. The Backward differentiation method is used in filtering application [31]. The difference equation of the low pass filter is,

$$y[k+1] = (1 - \Delta T \omega_c) y[k] + \Delta T \omega_c x[k] \tag{34}$$

Figure 4.18 shows the FFT of the signal before and after applying the low-pass filter. After applying the low-pass filter, the magnitude at 0.6 kHz is reduced from 0.571 to 0.012 nm.

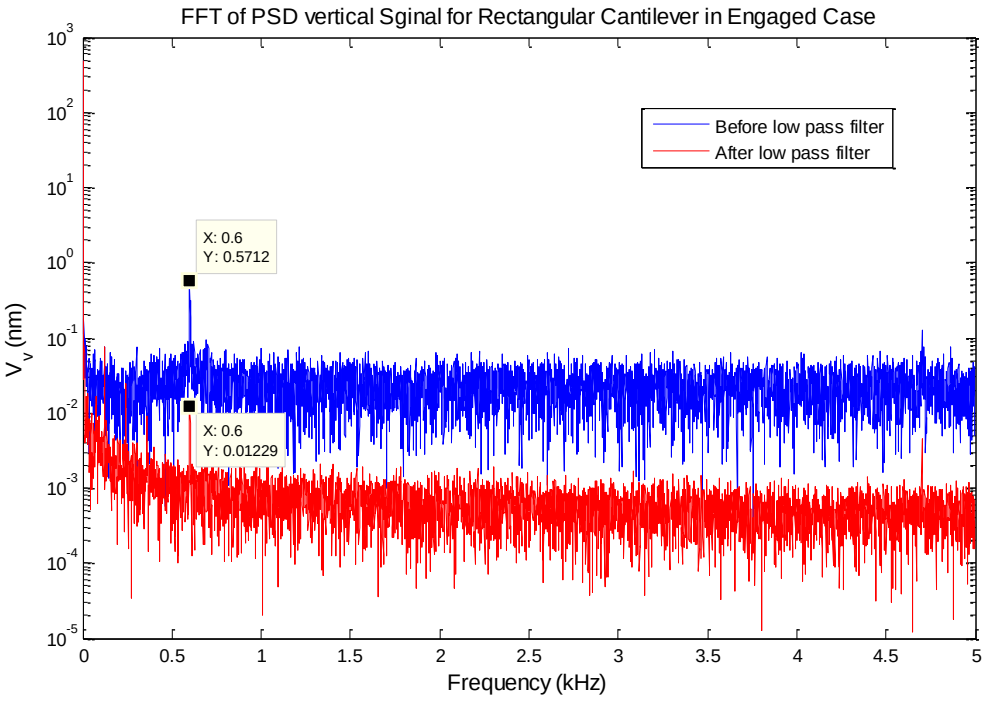

Figure 4.18 FFT of the photodiode vertical signal before and after applying the low pass filter

Figure 4.19 shows the result from applying the same filter to the photodiode signal. The difference between the maximum and minimum is 1.68 nm and 0.19 nm for the before and after applying the filter, respectively. Note that the picocube closed-loop resolution is 0.1 nm and the nano stage resolution is 0.2 nm. Therefore, The high freqancy force magnitudes were reduced after appling the low pass filter. Thus, the stylus' position has less high frequancy vibration from appling the filterd force. Consequently, the probe's tip has better interaction with the surface of the sample.

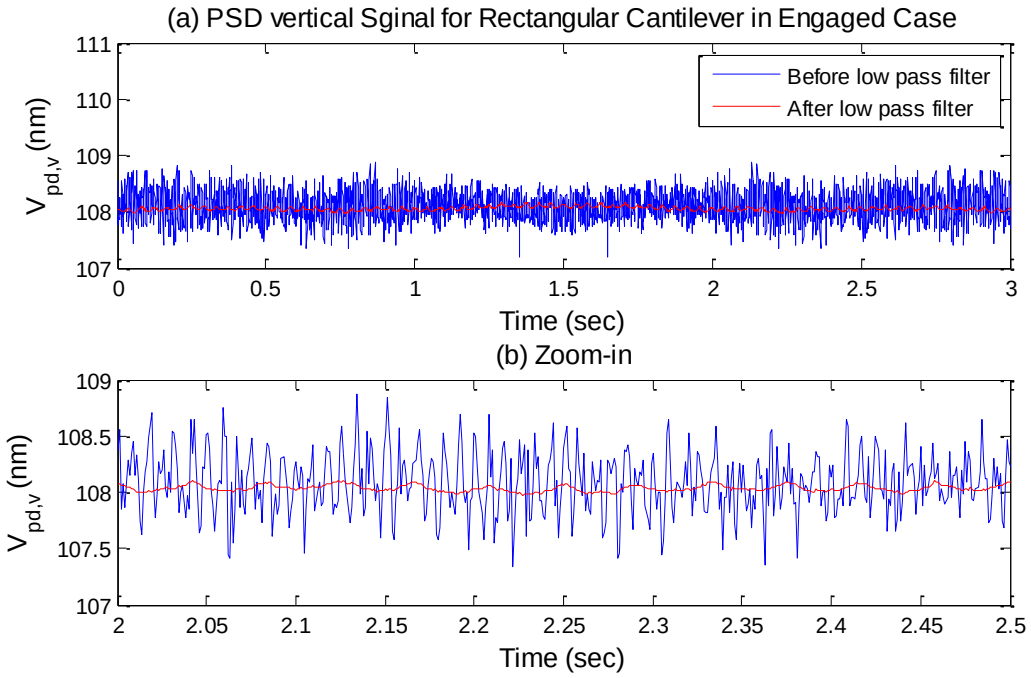

Figure 4.19 (a) Filtered photodiode vertical signal for 3 seconds while the tip engaged with sample and the picocube at a fixed position (b) Zoom-in for 0.5 sec

4.4. HAPTIC-PICOCUBE COUPLED MOTION

Testing the efficacy of the filter and calibration work is explained in this section. Testing the system after completing the work on each part of the haptic-AFM interface. This include of applying the low-pass filter, calibrating the normal gain, and calibrating the lateral gain on the test. Figure 4.20 shows the imaging of the sample's surface using the engagement of the cantilever with the sample while Figure 4.21 shows the haptic-picocube coupled motion that results from the interaction of the cantilever and the sample.

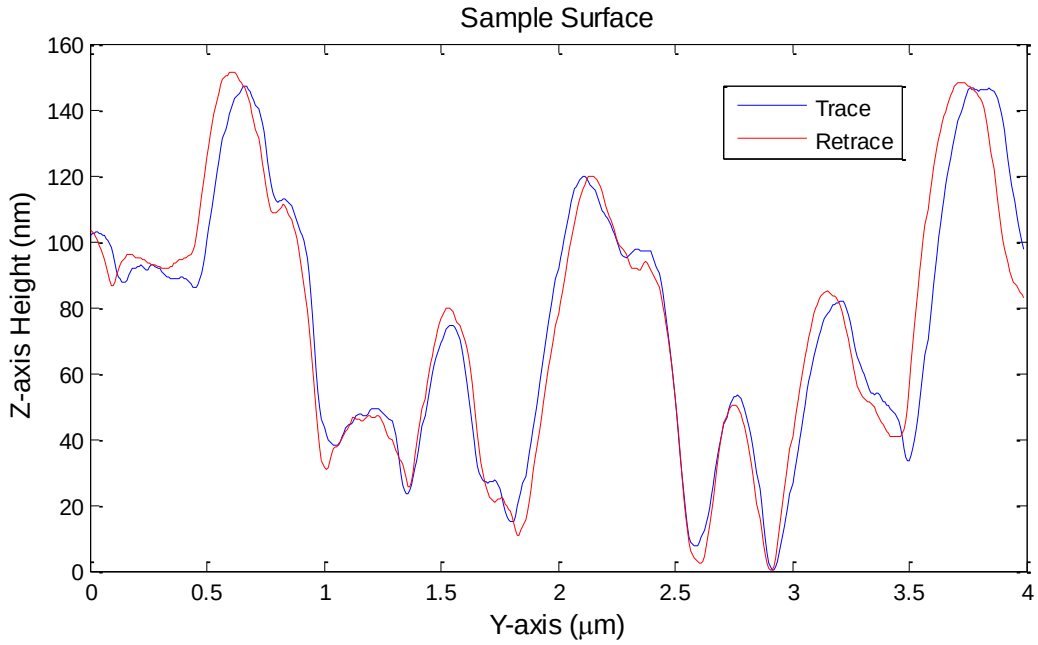

Figure 4.20 Sample surface from imaging mode for 4 μm length (magnetite sample)

Figure 4.20 shows the surface of a magnetite sample used to perform this test. This type of sample has a complex surface feature which is desirable for the user to feel the surface from the haptic. The height (in Z axis) of the sample feature varied between 20 nm and 150 nm while the image in Figure 4.20 has 4 μm length (in Y axis).

Figure 4.21 shows the result after engaging the probe tip with sample and coupling the haptic-picocube motion for 10 seconds. The first curve represents the position of the picocube on the Z-axis in nm for 200 nm range. The second curve shows the Z-axis force applied on the haptic in N. The picocube position on the Y-axis is shown in the third curve for 4 μm, and the Y-axis force acting on the haptic in N is on the last curve. The maximum normal force applied on the haptic was 1.73 N at 7.7 sec and -0.1770 N for the lateral force at 2.25 sec.

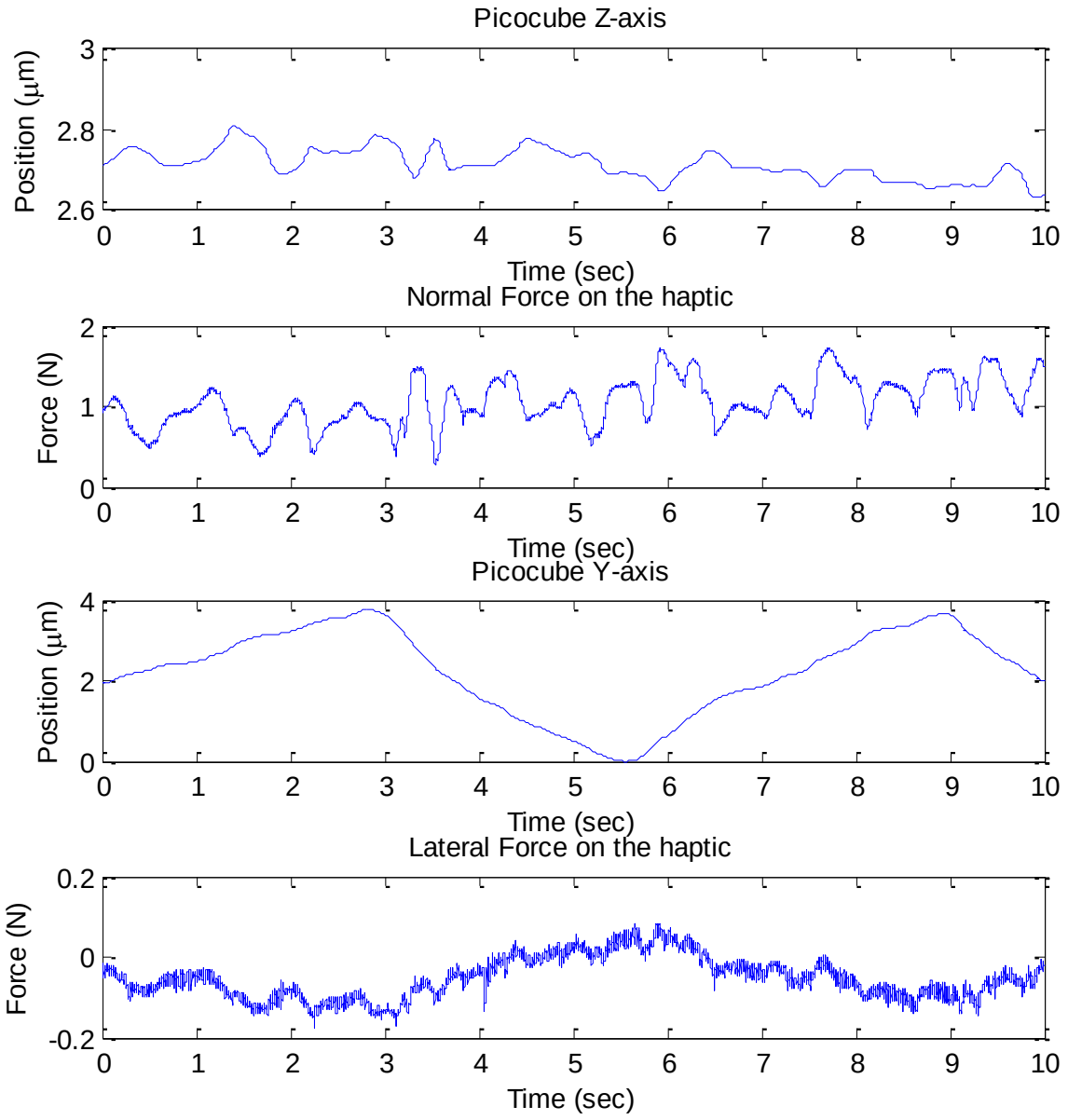

Fguire 4.21 Haptic-picocube coupled motion in YZ axes for 10 sec

The result in this section shows how the force feedback haptic device acts while the user is moving the stylus. When the probe tip reaches a high feature surface like in time equal to 1 sec, the cantilever starts to deflect and generate a normal force in Z direction that transmitted to the haptic. In time equal to 2 sec, the cantilever tip slide on the slope located at 3.5 to 4 µm in Y axis of the sample. This slope makes the cantilever to twist and to

generate a lateral force in the Y direction that transmitted to the haptic. As a result, the haptic-picocube coupled motion matches what is expected as the cantilever bends or twists and the force acts on the haptic due to these displacement from the cantilever.

5. CONCLUSION

A force-feedback haptic device is interfaced with an atomic force microscopy using contact mode cantilever. The experiment results provide the relationship between the forces and the input signal from the photodiode. Also, the motion sensitivity between the haptic and the cantilever from centimeter scale (haptic) to nano scale (cantilever).

This thesis provides a method of using a low-pass filter with the photodiode signal for obtaining better haptic behavior by cutting the high frequency noise coming from the system. Therefore, the haptics' stylus oscillation from the system noise is reduced, something which allows the user to feel closer to the interaction between the sample surface and probe tip. Consequently, the probe's tip has better interaction with the surface of the sample.

Calibrating the system is essential to perform a manipulation or investigation on the sample since the forces must be precise to obtain accurate results. The way that the experiment is set up in a precise manner provides desirable results. For example, the way that the laser is pointed at the end of the probe provides a situation where there will be greater sensitivity and the photodiode signal will be less noisy.

APPENDIX A

C CODE USED TO CREATE THE HAPTIC DEVICE DLL

A1 HEDAER FILE

```
//Header file (.h)

//Header files
#include <HD/hd.h>
#include <HDU/hduVector.h>
#include <HDU/hduError.h>

//Export functions
//Initializes the device, register Callback, start Scheduler
extern "C" __declspec(dllexport) int __cdecl initAndSchedule(HHD* phHD,
HDSchedulerHandle* pschedHand, double gPos[3]);

extern "C" __declspec(dllexport) void __cdecl setForce(double Xforce, double
Yforce, double Zforce);

extern "C" __declspec(dllexport) void __cdecl getPos(double *x, double *y, double
*z, int *Button);

//Stop and disable the device
extern "C" __declspec(dllexport) int __cdecl stopAndDisable(HHD hHD,
HDSchedulerHandle schedHand);
```

A2 MAIN FILE

```
//Main file (.cpp)

//Header files
#include "stdafx.h"
#include <cstdio>
#include <cassert>
#include <conio.h>
#include <windows.h>
#include "hapticHeader.h"

double gPos[3];
double gXforce;
double gYforce;
double gZforce;
int gButton;


//The device callback function
//Scheduler operation function type, used to define operations to be run in the
scheduler thread
extern "C" HDCallbackCode HDCALLBACK PositionCallback(void* pUserData)
{

       int nCurrentButtons;
       int nLastButtons;


       hdBeginFrame(hdGetCurrentDevice());

       hdGetIntegerv(HD_CURRENT_BUTTONS, &nCurrentButtons);
    hdGetIntegerv(HD_LAST_BUTTONS, &nLastButtons);

       if ((nCurrentButtons & HD_DEVICE_BUTTON_1) != 0 &&
        (nLastButtons & HD_DEVICE_BUTTON_1) == 0)
    {
        /* Detected button down */
             gButton=1;
    }
    else if ((nCurrentButtons & HD_DEVICE_BUTTON_1) == 0 &&
             (nLastButtons & HD_DEVICE_BUTTON_1) != 0)

    {
        /* Detected button up */
             gButton=0;
    }

    hduVector3Dd position;
    hduVector3Dd f;
       hduVector3Dd force(gXforce,gYforce,gZforce);
       f=force;

    hdSetDoublev(HD_CURRENT_FORCE, f);

    hdEndFrame(hdGetCurrentDevice()); //Ends the device frame ( Gets the handle of
the current device )
```

```
    HDErrorInfo error; //Intersperse in code to occasionally check for errors
        if (HD_DEVICE_ERROR(error = hdGetError()))
        {
            return HD_CALLBACK_DONE; //return HD_CALLBACK_DONE when it is finally
to be unscheduled.
        }



    hdGetDoublev(HD_CURRENT_POSITION,gPos);
    return HD_CALLBACK_CONTINUE; // returns HD_CALLBACK_CONTINUE to run
indefinitely, the application can call hdUnschedule() to force the callback to
terminate

}

/***********************************
INITANDSCHEDULE: Initializes the device, register Callback, start Scheduler.
***********************************/
__declspec(dllexport) int __cdecl initAndSchedule(HHD* phHD, HDSchedulerHandle*
pschedHand, double gPos[3])
{
    HDErrorInfo error;

    HHD hHD = hdInitDevice(HD_DEFAULT_DEVICE); //Initializes the device
(initialize the first device that it finds)

    if (HD_DEVICE_ERROR(error=hdGetError()))
    {
        return -1;
    }
       hdSetSchedulerRate(500);
    hdEnable(HD_FORCE_OUTPUT); //Enables a capability (Force output for the
device)

    //Schedules an operation to be executed by the scheduler in the servo loop
(The function callback,The data to be used by the function, The priority of the
operation)
    HDSchedulerHandle schedHand= hdScheduleAsynchronous(&PositionCallback,
0,HD_DEFAULT_SCHEDULER_PRIORITY);

    hdStartScheduler(); //Starts the scheduler. The scheduler manages callbacks to
be executed within the servo loop thread

    *phHD = hHD;
    *pschedHand = schedHand;
    return 1;
}

/***********************************
Get the position of the device
***********************************/
__declspec(dllexport) void __cdecl setForce(double Xforce, double Yforce, double
Zforce)
{
    gXforce=Xforce;
```

```
        gYforce=Yforce;
        gZforce=Zforce;
}


__declspec(dllexport) void __cdecl getPos(double *x, double *y, double *z, int
*Button)
{
    *x=gPos[0];
    *y=gPos[1];
    *z=gPos[2];
       *Button=gButton;
}


/*****************************
STOPANDDISABLE: Stop and disable the device
*****************************/
__declspec(dllexport) int __cdecl stopAndDisable(HHD hHD, HDSchedulerHandle
schedHand)
{
    hdStopScheduler(); //Typically call this as a first step for cleanup and
shutdown of devices
    hdUnschedule(schedHand); //Un-schedules an operation by removing the
associated callback from the scheduler
    hdDisableDevice(hHD); //Call during cleanup when done using a device.
Typically the last call after stopping the scheduler and unscheduling all
scheduled callbacks.

    return 1;
}
```

APPENDIX B

LABVIEW PROGRAMS USED IN THE EXPERIMENTS

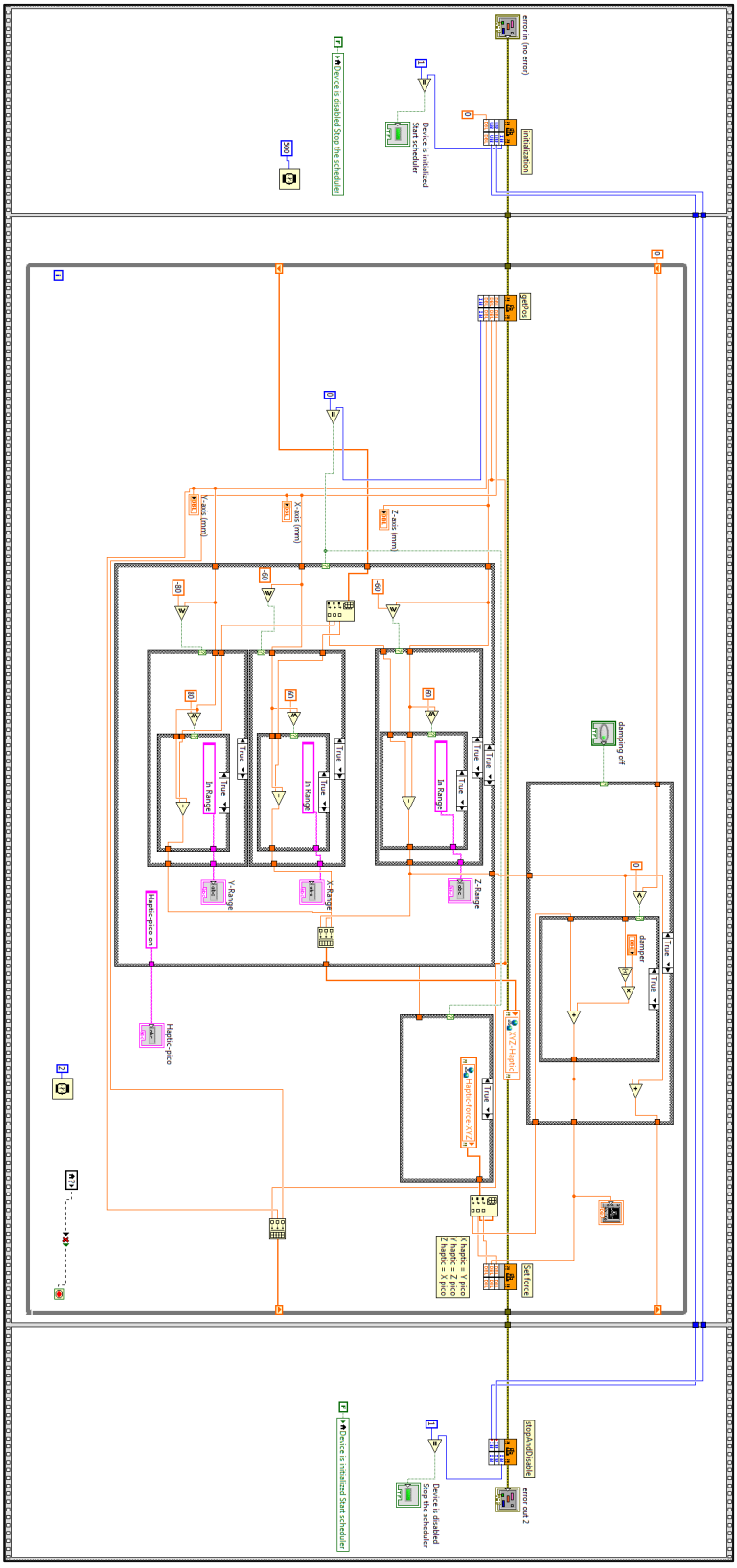

Figure B. 1. Haptic Host PC program

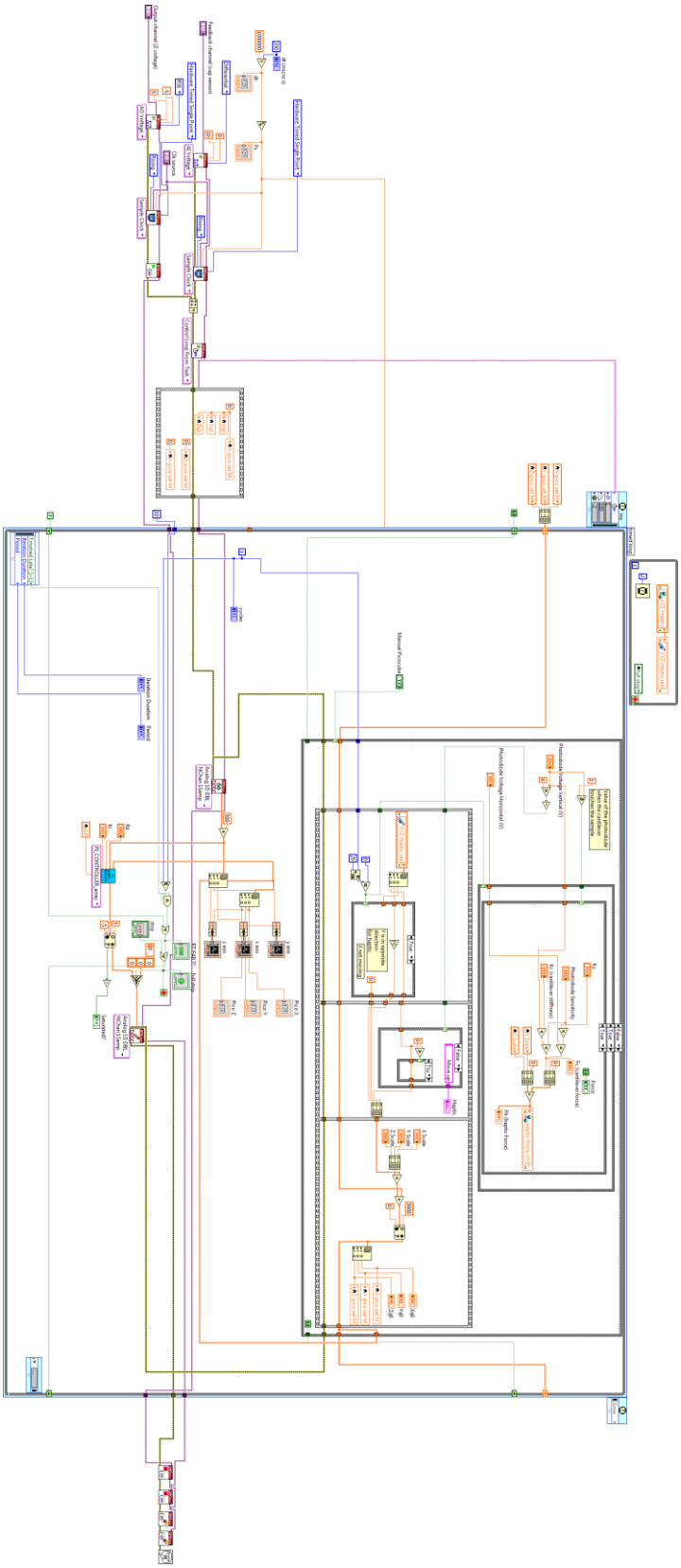

Figure B. 2. Haptic-picocube coupled motion program

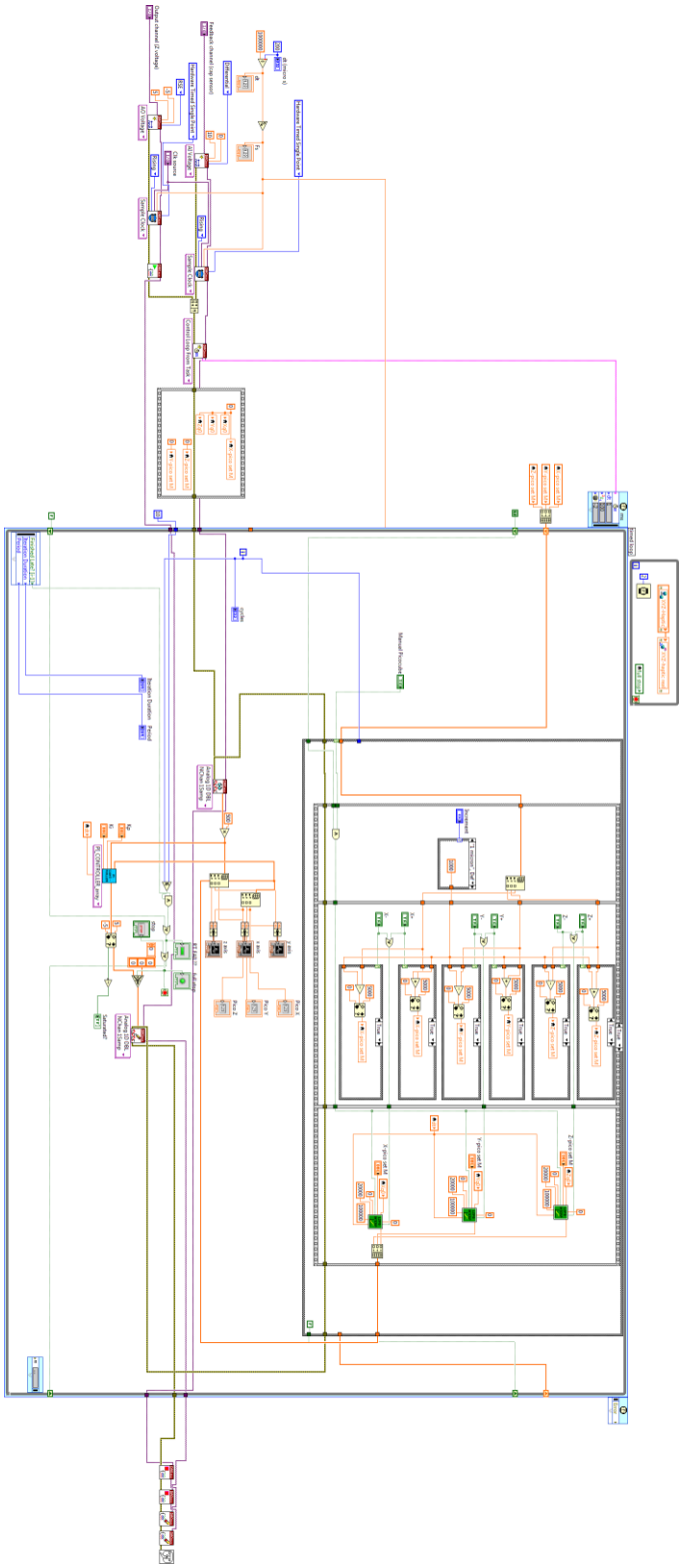

Figure B. 3. Picocube Jogs program

BIBLIOGRAPHY

1. Binnig, G., Quate, C. F., & Gerber, C. (1986). Atomic force microscope.*Physical review letters*, *56*(9), 930.

2. Mosher, R.S.: Industrial Manipulators. Scientific American (1964). 211(4). 88-(1968) NASA, Washington DC, Ref. NASA SP-5070.

3. Corliss, W.R., and Johnson, E.G.: Teleoperator Controls. AEC-NASA Technology Survey.

4. Thring, M.W.: Robots and Telechirs. Ellis Horwood, Chichester (1983).

5. Sitti, M., & Hashimoto, H. (1998, October). Tele-nanorobotics using atomic force microscope. In *Intelligent Robots and Systems, 1998. Proceedings., 1998 IEEE/RSJ International Conference on* (Vol. 3, pp. 1739-1746). IEEE.

6. Guthold, M., Falvo, M. R., Matthews, W. G., Paulson, S., Washburn, S., Erie, D. A., ... & Taylor, R. M. (2000). Controlled manipulation of molecular samples with the nanomanipulator. *Mechatronics, IEEE/ASME Transactions on*, *5*(2), 189-198.

7. Li, G., Xi, N., Yu, M., & Fung, W. K. (2003, August). Augmented reality system for real-time nanomanipulation. In *Nanotechnology, 2003. IEEE-NANO 2003. 2003 Third IEEE Conference on* (Vol. 1, pp. 64-67). IEEE.

8. Massie, T. H., & Salisbury, J. K. (1994, November). The phantom haptic interface: A device for probing virtual objects. In *Proceedings of the ASME winter annual meeting, symposium on haptic interfaces for virtual environment and teleoperator systems* (Vol. 55, No. 1, pp. 295-300).

9. Li, G., Xi, N., Yu, M., & Fung, W. K. (2004). Development of augmented reality system for AFM-based nanomanipulation. *Mechatronics, IEEE/ASME Transactions on*, *9*(2), 358-365.

10. Li, G., Xi, N., & Yu, M. (2004, April). Calibration of AFM based nanomanipulation system. In *Robotics and Automation, 2004. Proceedings. ICRA'04. 2004 IEEE International Conference on* (Vol. 1, pp. 422-427). IEEE.

11. Liu, E., Blanpain, B., & Celis, J. P. (1996). Calibration procedures for frictional measurements with a lateral force microscope. *Wear*, *192*(1), 141-150.

12. Cain, R. G., Biggs, S., & Page, N. W. (2000). Force calibration in lateral force microscopy. *Journal of colloid and interface science*, *227*(1), 55-65.

13. Ogletree, D. F., Carpick, R. W., & Salmeron, M. (1996). Calibration of frictional forces in atomic force microscopy. *Review of Scientific Instruments*, *67*(9), 3298-3306.

14. Liu, L., Jiao, N., Tian, X., Dong, Z., Xi, N., Li, W. J., & Wang, Y. (2006, January). Development of a haptic user interface for surface sensing and nanomanipulation based on atomic force microscope. In *Nano/Micro Engineered and Molecular Systems, 2006. NEMS'06. 1st IEEE International Conference on* (pp. 900-904). IEEE.

15. Zhang, J., Xi, N., Li, G., Chan, H. Y., & Wejinya, U. C. (2006). Adaptable end effector for atomic force microscopy based nanomanipulation. *Nanotechnology, IEEE Transactions on*, *5*(6), 628-642.

16. Guthold, M., Falvo, M. R., Matthews, W. G., Paulson, S., Washburn, S., Erie, D. A., ... & Taylor, R. M. (2000). Controlled manipulation of molecular samples with the nanomanipulator. *Mechatronics, IEEE/ASME Transactions on*, *5*(2), 189-198.

17. Vogl, W., Ma, B. K. L., & Sitti, M. (2006). Augmented reality user interface for an atomic force microscope-based nanorobotic system. *Nanotechnology, IEEE Transactions on*, *5*(4), 397-406.

18. Zhang, J., Xi, N., Li, G., Chan, H. Y., & Wejinya, U. C. (2006). Adaptable end effector for atomic force microscopy based nanomanipulation. *Nanotechnology, IEEE Transactions on*, *5*(6), 628-642.

19. Iwata, F., Ohara, K., Ishizu, Y., Sasaki, A., Aoyama, H., & Ushiki, T. (2008). Nanometer-scale manipulation and ultrasonic cutting using an atomic force microscope controlled by a haptic device as a human interface. *Japanese Journal of Applied Physics*, *47*(7S2), 6181.

20. "Compact Micro-Translation Stage," http://www.physikinstrumente.com/product-detail-page/m-110-m-111-m-112-701650.html, 2015.

21. "PIHera XY Piezo Stage," http://www.physikinstrumente.com/product-detail-page/p-6202-p-6292-202400.html, 2015.

22. "PIHera Precision Z-Stage," http://www.physikinstrumente.com/product-detail-page/p-620z-p-622z-202500.html, 2015.

23. Geomagic Touch X Device Guide.

24. OpenHaptics Programmer's Guide.

25. OpenHaptics API Reference.

26. "Lessard, C., & Falcon, J., 2014 Tips for Code Re-Use," ftp://ftp.ni.com/pub/branches/india/tips_for_code_re_use2014.pdf, 2014.

27. “Supported Data Types for the Import Shared Library Wizard,” http://zone.ni.com/reference/en-XX/help/371361J-01/lvexcodeconcepts/supp_data_importdllwiz/, 2015.

28. “C/C++ DLL Call Parameters,” http://zone.ni.com/reference/en-XX/help/370052H-01/tsref/infotopics/db_editdllcall_numparam/, 2015.

29. “TOP VISUAL CONTACT Silicon Cantilevers VIT_P_C-A series,” http://www.ntmdt-tips.com/products/view/vit-p-c-a, 2015.

30. Lindeke, R., “Path Control in Robotics,” http://www.d.umn.edu/~rlindek1/Robotics/Class_Matls/Robotic%20Path%20Control%20Techniques.ppt, 2015.

31. Haugen, F. (2008). Derivation of a Discrete-Time Lowpass Filter.

32. Brooks, T. L. (1990, November). Telerobotic response requirements. In*Systems, Man and Cybernetics, 1990. Conference Proceedings., IEEE International Conference on* (pp. 113-120). IEEE.

VITA

Abdulmohsen Alabdulmuhsin was born in Riyadh, Saudi Arabia on May 27th, 1988. He obtained his Bachelor's degree in Mechanical Engineering (University rank: 1/244) on May 2010 from King Saud University, Riyadh, Saudi Arabia.

He joined Missouri University of Science and Technology in the spring 2014 semester to pursue his Masters in Mechanical Engineering with a specialization in Control Systems. He worked in the Precision Motion Control Lab (PMCL) at Missouri S&T under Dr. Douglas Bristow. He received his Master of Science degree in August 2015.